J. Fluid Mech. (2017), *vol.* 830, *pp.* 408–438. © Cambridge University Press 2017
doi:10.1017/jfm.2017.593

Spectral analysis and coherence of aerodynamic lift on rectangular cylinders in turbulent flow

Shaopeng Li[1,†] **and Mingshui Li**[2,†]

[1]School of Civil Engineering, Key Laboratory of New Technology for Construction of Cities in Mountain Area, Chongqing University, Chongqing 400045, PR China

[2]Research Centre for Wind Engineering, Southwest Jiaotong University, Chengdu 610031, PR China

(Received 11 August 2016; revised 9 August 2017; accepted 17 August 2017;
first published online 3 October 2017)

The goal of the present work is to derive the closed-form expressions of coherence and admittances to describe the spatial distribution of lift on rectangular cylinders in turbulent flow, which can be used to investigate the three-dimensional effects of turbulence. The coherence of the three-dimensional aerodynamic admittance (3D AAF), which takes into full account the spanwise variations in the vertical velocity fluctuations, is introduced to assess the validity of the strip assumption. A theoretical coherence model expressed in a double-exponential form is derived starting from the two-wavenumber spectral tensor of the lift on a thin aerofoil in Fourier space, providing us with explicit insight into the coherence of the lift force. Notably, it is an intrinsic property that the lift force on the structure is more strongly correlated than the oncoming flow and 3D AAF. This coherence model is extended to rectangular cylinders by the introduction of three floating parameters into the decay parameters of the 3D AAF. Based on theoretical and experimental investigations, it is shown that the three-dimensional effects of turbulence grow more prominent as the difference between the decay parameters of the 3D AAF and vertical velocity fluctuations decreases. A generalized approach for rapidly deriving the closed-form expressions of the admittances is proposed to study the unsteady behaviour of the lift force and the distortion of the free stream passing through the rectangular cylinders.

Key words: aerodynamics, flow–structure interactions, turbulent flows

1. Introduction

Spatial distribution, particularly that of coherence and aerodynamic admittance, is of great importance for understanding the unsteady behaviour of the lift on structures in turbulent flow. The structures concerned in this respect include the aerofoil as well as a number of bluff bodies, such as bridge decks, turbine blades, and tall buildings. A key point of study is the description of the three-dimensional spectral tensor of the lift in Fourier space and the derivation of analytical solutions for coherence and admittances that retain most of the structural information regarding the three-dimensional effects of turbulence. The usual starting point for

† Email addresses for correspondence: lishaopeng0314@163.com, lms_rcwe@126.com

the above-mentioned three-dimensional effects is to study the spanwise correlation of the lift. In practical gust-loading problems, a strip-theory assumption (Fung 1969) is usually adopted wherein the spatial correlation of the turbulence is used to describe the three-dimensional properties of the lift force. It is well known that the strip-theory assumption becomes more accurate as the length scale of the turbulence increases. However, published experimental studies (Etkin 1971; Hjorth-Hansen, Jakobsen & Strømmen 1992; Sankaran & Jancauskas 1993; Jakobsen 1997; Kimura *et al.* 1997; Larose 1997; Larose & Mann 1998; Ma 2007; Ito, Shirato & Matsumoto 2014; Li 2015; Li, Li & Liao 2015; Hann, Wu & Kareem 2016; Yan, Zhu & Flay 2016) show that the spanwise correlation of the lift force is greater than that of the turbulence when the length scale of the oncoming flow is not large compared with the characteristic length of the body (Taylor 1965). In fact, the three-dimensional effects of the turbulence rely on the exact description of the aerodynamic admittance in the spectral tensor of the lift, as the aerodynamic admittance is generally regarded as the aerodynamic transfer function of a linear time-invariant system.

Early relevant studies primarily focused on the lift behaviour on an aerofoil. Using the strip assumption, Sears' linearized spectral model of lift on a thin strip was expressed in terms of two-dimensional aerodynamic admittance (2D AAF), the Sears' function. Liepmann (1955) extended this two-dimensional spectral model to a three-dimensional one by introducing the 3D AAF, $\chi_L(k_1, k_2)$, which was defined as the two-dimensional Fourier transform of the indicial admittance $h(t, y)$. Such a 3D spectral model can better account for the three-dimensional nature of turbulence with respect to the spanwise direction of a finite aerofoil. A more general admittance model was proposed by Ribner (1956) using the three-wavenumber spectral tensor. Based on lifting-surface theory, a 3D AAF described by two wavenumbers, chordwise and spanwise, was developed to theoretically study the unsteady lift on a thin aerofoil in a two-dimensional sinusoidal flow field (Filotas 1969*a*,*b*; Graham 1970, 1971). Graham's 3D AAF was experimentally validated by Jackson, Graham & Maull (1973) indirectly. In a previous paper (Li *et al.* 2015), we developed a general approach numerically determining the two-wavenumber spectrum and admittance of the lift on a thin aerofoil in grid-generated turbulence, which is highly accurate compared with Sears' and Graham's theoretical results. It should be noted that the above-mentioned approach can be applied to bluff bodies with complex cross-sectional shapes. In the present paper, we extend this work from a numerical solution to an analytical solution, following Ribner's three-dimensional theory.

Because of the complex separation of flow, it is known that potential theory certainly fails to account for the spatial characteristics of lift on bluff bodies, such as rectangular cylinders and streamlined bridge decks. This problem is a classic one that has attracted considerable attention. In previous studies, empirical spectral models of the lift were proposed in terms of the generalized one-wavenumber admittance and the coherence of the lift based on experimental investigations. In contrast with the 3D AAF, the generalized one-wavenumber admittance is unable to describe the effects of spanwise variations of turbulence on the spatial lift distribution on bluff bodies. In addition, while a series of empirical coherence models were obtained, the nature of the coherent structure of the lift remained unclear as these models were developed simply by modifying the turbulence models proposed by Davenport (1962) in a simple exponential form or those proposed by Roberts & Surry (1973) and Irwin (1977) in terms of Bessel functions. Therefore, it is necessary to present an approximate closed solution for the spatial lift distribution, including coherence and admittances, to explicitly interpret the three-dimensional effects of the turbulence.

Generally, we know that body-induced vortex shedding may affect the flow separation and coherence of lift within a certain frequency band (frequency of Kármán vortex street). Moreover, the spectral and coherence proposed herein do not take this effect into consideration. This simplification is acceptable from the viewpoint of calculating the buffeting response, because the frequency of the vortex shedding is usually much higher than the natural frequency of the line-like structures encountered in practical engineering.

The aim of the present work is to propose a generalized approach based on Ribner's three-dimensional theory, yielding closed-form expressions for the coherence and admittances of lift on rectangular cylinders in turbulent flow. Three steps are required in such an approach. In the first step, a more tractable coherence model must be derived in Fourier space by parametrizing the coherence of the lift in terms of the coherence of the 3D AAF and vertical velocity fluctuations. The second step is to present closed-form expressions of lift admittances using the proposed coherence model, after which the three-dimensional effects of the turbulent flow can be studied by means of a second-order spectral tensor method. The third step is to mathematically quantify the effects of the decay parameters of the 3D AAF and vertical velocity fluctuations on the spanwise correlation of lift. The model developed in the present paper can be used to describe the spatial distribution of lift on line-like structures with bluff cross-section shapes in turbulent flow. Using a series of wind tunnel tests, these models have been validated and thus allow us to investigate the spatial correlation of lift on bodies in turbulent flow from an energy-transition point of view.

2. Mathematical model

In this section, the model that describes the lift coherence on an aerofoil is derived theoretically using Ribner's three-dimensional theory outlined in § 2.1. The model can be extended to rectangular cylinders by defining three constant coefficients in the decay parameter of the 3D AAF, as described in § 2.2.1. In § 2.2.2, a closure method for obtaining approximate expressions of the admittances is proposed using the proposed coherence model. In § 2.3, the effects of the decay parameters (corresponding to vertical velocity fluctuations and 3D AAF) on the spanwise correlation of the lift force are studied in detail.

2.1. *Theoretical coherence model of the lift force on a thin aerofoil*

The three-dimensional spectral tensor model proposed by Ribner (1956) is reviewed for the sake of clarity, which is defined as

$$S_L(\boldsymbol{k}) = (\rho U b C_L')^2 |\chi_L(\boldsymbol{k})|^2 S_w(\boldsymbol{k}), \tag{2.1}$$

where ρ, U, b and C_L' are, respectively, the air density, mean wind velocity, the semi-chord length of aerofoil and the lift slope, $\boldsymbol{k}$ is a wavevector with three components k_1, k_2 and k_3 as the wavenumbers in the x, y and z directions, respectively (see figure 1), $k_i = n_i/U$ (n_i is frequency), $|\chi_L(\boldsymbol{k})|^2$ is the three-wavenumber aerodynamic admittance, and $S_w(\boldsymbol{k})$ is the three-wavenumber spectrum of vertical velocity fluctuations (see § A.1).

The present study focuses on investigating the lift coherence on bodies whose geometrical dimensions in the z direction are far smaller than those in the other two directions, such as aerofoils, flat plates and long span bridge decks. In this case, the lift force on the body is sensitive only to the turbulence pattern in the (x, y) plane (Jackson *et al.* 1973). Hence, k_3 can be integrated out in (2.1), resulting in a reduction to two dimensions: the (x, y) plane (Ribner 1956). The method for obtaining

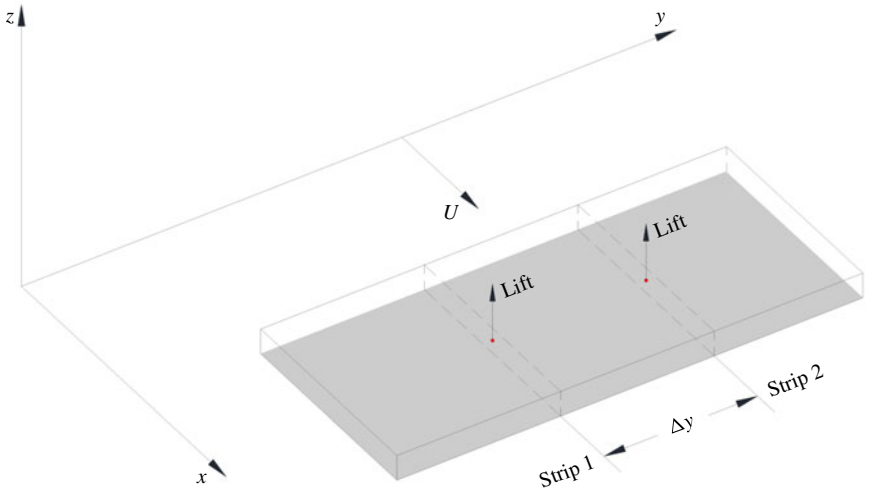

FIGURE 1. (Colour online) The coordinate system features an x-axis in the direction of the mean wind U, a y-axis along the span of the body, and a z-axis perpendicular to the other two axes.

the cross-spectrum of the lift on an aerofoil is described in detail in § A.2, which is given by

$$S_L(k_1, \Delta y) = (\rho U b C_L')^2 [|\chi_L(k_1, \Delta y)|^2 \otimes \mathrm{Coh}_w(k_1, \Delta y)] S_w(k_1), \tag{2.2}$$

where $|\chi_L(k_1, \Delta y)|^2$ is defined as the cross-3D admittance, and $\mathrm{Coh}_w(k_1, \Delta y)$ and $S_w(k_1)$ correspond to the coherence and one-point spectrum of the vertical velocity fluctuations, respectively. The cross-3D admittance $|\chi_L(k_1, \Delta y)|^2$ can be obtained by using the inverse Fourier transform of Graham's two-wavenumber aerodynamic admittance (Graham 1970, 1971). However, Graham's function is a numerical solution. Therefore, it is difficult to apply to derive the closed solution for $|\chi_L(k_1, \Delta y)|^2$. Instead, the approximate formulae for the 3D AAF of lift on a thin aerofoil are presented as correction factors to Sears' function (Mugridge 1970, 1971; Blake 1986) in §§ B.1 and B.2. By defining the coherence of 3D AAF $\mathrm{Coh}_{\chi_L}(k_1, \Delta y)$, the approximate expression for $|\chi_L(k_1, \Delta y)|^2$ is as indicated in § B.3.

With respect to $\mathrm{Coh}_w(k_1, \Delta y)$, Irwin (1977) proposed a theoretical model for homogeneous isotropic turbulence based on the von Kármán spectrum. However, Irwin's coherence model is represented in terms of Bessel functions, which can hardly be applied to derive the closed-form expression of $S_L(k_1, \Delta y)$ in (2.2). The modified exponential coherence model proposed by Jakobsen (1997) is more feasible. However, because of its dimension-dependent feature, Jakobsen's empirical model is also limiting. By non-dimensionalizing this expression, the improved formula is as presented in appendix C.

Substituting (B 5)–(B 6) and (C 1)–(C 2) into (2.2), the closed-form expression of $S_L(k_1, \Delta y)$, considering the three-dimensionality of the turbulence, can be derived mathematically via a convolution operation:

$$\begin{aligned} S_L(k_1, \Delta y) &= (\rho U b C_L')^2 \left[\int_{-\infty}^{\infty} |\chi_L(k_1, \tau)|^2 \, \mathrm{Coh}_w(k_1, \Delta y - \tau) \, \mathrm{d}\tau \right] S_w(k_1) \\ &= (\rho U b C_L')^2 \Psi_L(k_1, \Delta y) S_w(k_1), \end{aligned} \tag{2.3}$$

where

$$\Psi_L(k_1, \Delta y) = \frac{1}{1+2\pi\tilde{k}_1}\left[\frac{\lambda_L^2 \exp(-2\pi A_w \Delta y) - \lambda_L A_w \exp(-2\pi\lambda_L \Delta y)}{\lambda_L^2 - A_w^2}\right] \tag{2.4}$$

and $\Psi_L(k_1, \Delta y)$ is defined as the equivalent coherence of the lift force, which can be used to describe the effects of three-dimensional turbulence and 3D AAF on the spatial distribution of the lift force on a thin aerofoil, λ_L and A_w are the decay parameters corresponding to the coherence of the 3D AAF and vertical velocity fluctuations, respectively. If we set $\Delta y = 0$, the one-point spectrum of the lift can be derived from (2.3)–(2.4) as

$$S_L(k_1) = (\rho U b C_L')^2 |\chi_L(k_1)|^2 S_w(k_1), \tag{2.5}$$

where $|\chi_L(k_1)|^2$ is the generalized one-wavenumber admittance in terms of the two-dimensional aerodynamic admittance and the spanwise correction factor in (B 1), defined by

$$|\chi_L(k_1)|^2 = \underbrace{\frac{1}{1+2\pi\tilde{k}_1}}_{\textit{Sears' fun.}} \underbrace{|F_L(k_1)|^2}_{\textit{correction fac.}}, \tag{2.6}$$

with

$$|F_L(k_1)|^2 = \frac{\lambda_L}{\lambda_L + A_w} \tag{2.7}$$

is the one-dimensional correction factor of $|\chi_L(k_1)|^2$. The validation of the proposed closed-form expression of the cross-spectrum of the lift is presented in detail in appendix D.

The coherence of the lift force on a thin aerofoil is defined as

$$\mathrm{Coh}_L(k_1, \Delta y) = \frac{S_L(k_1, \Delta y)}{S_L(k_1)}. \tag{2.8}$$

Substituting (2.3)–(2.7) into (2.8), the closed-form expression of the lift coherence is given by

$$\mathrm{Coh}_L(k_1, \Delta y) = \frac{\lambda_L \exp(-2\pi A_w \Delta y) - A_w \exp(-2\pi\lambda_L \Delta y)}{\lambda_L - A_w}. \tag{2.9}$$

Compared with previous coherence models (Hjorth-Hansen *et al.* 1992; Jakobsen 1997; Kimura *et al.* 1997; Larose & Mann 1998), the proposed expression is of physical significance and can describe the coherent structure of the lift along the y direction. Interestingly, equation (2.9) indicates that the spanwise correlation of the lift on a thin aerofoil is closely associated with that of the vertical velocity fluctuations and 3D AAF together. We can therefore quantitatively analyse the effects of the cross-sectional shapes of bodies and the three-dimensionality of turbulence on the spanwise correlation of the lift force (see § 2.3). The two-wavenumber coherence of the lift force can be obtained by taking the Fourier transform of (2.9), which yields

$$\Phi_L(k_1, k_2) = \frac{1}{\pi}\frac{\lambda_L A_w(\lambda_L + A_w)}{(\lambda_L^2 + k_2^2)(A_w^2 + k_2^2)}. \tag{2.10}$$

Substituting (2.5)–(2.7) into (2.8), the cross-spectrum of the lift force can be expressed as

$$S_L(k_1, \Delta y) = (\rho U b C_L')^2 |\chi_L(k_1)|^2 S_w(k_1)\,\mathrm{Coh}_L(k_1, \Delta y). \tag{2.11}$$

It should be noted that (2.11) is consistent with the gust-loading model proposed by Larose & Mann (1998). By comparing (2.3) with (2.11), the following relation can be obtained:

$$\Psi_L(k_1, \Delta y) = |\chi_L(k_1)|^2 \, \mathrm{Coh}_L(k_1, \Delta y). \tag{2.12}$$

As shown in (2.12), it is clear that the equivalent coherence of the lift can be expressed in terms of the generalized one-wavenumber admittance and the coherence of the lift force.

2.2. *Closed solution for the 3D AAF of a rectangular cylinder*

In this section, extensions of the presented lift coherence model to bluff bodies are made to quantitatively study the effects of three-dimensional flow (see § 2.3). We propose a general approach for obtaining the closed solution of the 3D AAF based on Ribner's three-dimensional theory.

2.2.1. *Extension of the proposed coherence model to a rectangular cylinder*

Despite its simple geometry, the three-dimensional flow over an elongated rectangular cylinder is highly complex because of the unsteady flow separation and reattachment that result in the three-dimensional spatial distribution of the unsteady lift force. Moreover, the structures with a rectangular cross-section are widely used in engineering. Thus, a rectangular cylinder is taken as the typical representation of a bluff body in the present paper. In this case, Graham's 3D AAF is certainly invalid because of the effects of flow separation and reattachment. Hence, the proposed coherence model cannot be applied directly. However, equation (2.9) is still of interest in investigating the coherent structure of the lift along the span, noting that the spanwise correlation of lift is mainly determined by the decay parameters of the 3D AAF and vertical velocity fluctuations. In fact, similarly to the spanwise distribution of the lift on a thin aerofoil, that of the lift on a slender body depends on the cross-sectional shape (associated with 3D AAF) and the spatial variations of the vertical velocity fluctuations. Therefore, for a given turbulent flow field, it is reasonable to assume that the double-exponential function (2.9) can be applied to describe the spanwise correlation of lift on a rectangular cylinder by appropriately modifying the decay parameter of the 3D AAF, λ_L^r. Thus, according to Mugridge's or Blake's expression, the present coherence model can be adjusted by defining λ_L^r as a function of three floating parameters as follows:

$$\mathrm{Coh}_L^r(k_1, \Delta y) = \frac{\lambda_L^r \exp(-2\pi A_w \Delta y) - A_w \exp(-2\pi \lambda_L^r \Delta y)}{\lambda_L^r - A_w}, \tag{2.13}$$

with

$$\lambda_L^r = \sqrt{a_1 (2\pi b k_1)^{a_2} + a_3}/(2\pi b), \tag{2.14}$$

where a_1, a_2 and a_3 are floating parameters that must be determined by wind tunnel tests. It should be noted that the coherence of the vertical velocity fluctuations is still described by Jakobsen's empirical model. In addition, the Fourier transform of (2.13) is simply a modified version of (2.9), replacing λ_L with λ_L^r.

2.2.2. *Closed-form expressions of admittances*

To obtain a closed-form expression for the three-dimensional aerodynamic admittance of lift on a rectangular cylinder, Ribner's theory can be applied. The

derivation procedure involves the following four steps:

(i) *Definition of the spectral model of the lift.* The three-dimensional spectrum of the lift acting on a rectangular cylinder should be defined first. This study adopts the following two-wavenumber spectral model proposed by Li *et al.* (2015):

$$S_L(k_1, k_2) = (\rho U b)^2 |\chi_L^r(k_1, k_2)|^2 [4C_L^2 S_u(k_1, k_2) + (C_L' + C_D)^2 S_w(k_1, k_2)], \tag{2.15}$$

where C_L and C_D are the lift and drag coefficients respectively, $S_u(k_1, k_2)$ is the two-wavenumber spectrum of longitudinal velocity fluctuations, and $|\chi_L^r(k_1, k_2)|^2$ is the 3D AAF. For simplicity, the contribution of the longitudinal velocity fluctuations to the lift on a rectangular cylinder can be neglected when the angle of attack of the incoming flow is zero. The equation (2.15) can thus be reduced to

$$S_L(k_1, k_2) = (\rho U b)^2 (C_L' + C_D)^2 |\chi_L^r(k_1, k_2)|^2 \Phi_w(k_1, k_2) S_w(k_1). \tag{2.16}$$

Therefore, the one-point spectrum of the lift can be obtained by integrating (2.16) over k_2 (see (D 1)). We thus have

$$S_L(k_1) = (\rho U b)^2 (C_L' + C_D)^2 |\chi_L^r(k_1)|^2 S_w(k_1), \tag{2.17}$$

where

$$|\chi_L^r(k_1)|^2 = \int_{-\infty}^{\infty} |\chi_L^r(k_1, k_2)|^2 \Phi_w(k_1, k_2)\, \mathrm{d}k_2. \tag{2.18}$$

Taking the Fourier transform of (2.8) and combining it with (2.17), the two-wavenumber spectrum of the lift can be rewritten as

$$S_L(k_1, k_2) = (\rho U b)^2 (C_L' + C_D)^2 |\chi_L^r(k_1)|^2 \Phi_L(k_1, k_2) S_w(k_1). \tag{2.19}$$

By comparing (2.16) with (2.19), the following relation can be obtained

$$\frac{|\chi_L^r(k_1, k_2)|^2}{|\chi_L^r(k_1)|^2} = \frac{\Phi_L(k_1, k_2)}{\Phi_w(k_1, k_2)}. \tag{2.20}$$

The relation described by (2.20) demonstrates the dependence of the admittances, including $|\chi_L^r(k_1, k_2)|^2$ and $|\chi_L^r(k_1)|^2$, on the spatial correlation of the lift and vertical velocity fluctuations. This relation will play an important role in the following derivation processes.

(ii) *Definition of 3D AAD and generalized one-wavenumber admittance.* Similarly to the thin aerofoil case, Li (2015) found that the admittance of the lift on a bluff body in two-dimensional flow (2D AAF), $|\chi_L^r(k_1, 0)|^2$, is a function of the reduced frequency $\tilde{k}_1 (= 2\pi k_1 b)$, known as Sears' function, and depends only on the cross-sectional shape. In analogy with (B 1), we therefore propose an approximate expression for formulating the 3D AAF of lift on a rectangular cylinder as follows:

$$|\chi_L^r(k_1, k_2)|^2 = |\chi_L^r(k_1, 0)|^2 |F_L^r(k_1, k_2)|^2, \tag{2.21}$$

where $|F_L^r(k_1,\ k_2)|^2$ is the correction factor to the two-dimensional admittance $|\chi_L^r(k_1, 0)|^2$. It should be noted that (2.21) will be reduced to 2D AAF for transversely

fully correlated gusts (when $k_2 = 0$). In this case, the correction factor $|F_L^r(k_1, k_2)|^2$ at $k_2 = 0$ satisfies

$$|F_L^r(k_1, 0)|^2 \equiv 1. \tag{2.22}$$

Substituting (2.21) into (2.18) results in the following generalized one-wavenumber admittance

$$|\chi_L^r(k_1)|^2 = |\chi_L^r(k_1, 0)|^2 |F_L^r(k_1)|^2, \tag{2.23}$$

where $|F_L^r(k_1)|^2$ represents the correction factor defined by

$$|F_L^r(k_1)|^2 = \int_{-\infty}^{\infty} |F_L^r(k_1, k_2)|^2 \Phi_w(k_1, k_2)\, \mathrm{d}k_2. \tag{2.24}$$

Similarly, the generalized one-wavenumber admittance can also be represented as a correction factor to the 2D AAF as shown in (2.21).

(iii) *Theoretical derivation of* $|F_L^r(k_1)|^2$. Substituting (2.21) and (2.23) into (2.20), the following relation can be obtained:

$$|F_L^r(k_1, k_2)|^2 \Phi_w(k_1, k_2) = |F_L^r(k_1)|^2 \Phi_L(k_1, k_2). \tag{2.25}$$

Given that $k_2 = 0$ and using (2.22), the correction factor of the generalized one-wavenumber admittance is given by

$$|F_L^r(k_1)|^2 = \frac{\Phi_w(k_1, 0)}{\Phi_L(k_1, 0)}. \tag{2.26}$$

Substituting (C 3) and (2.10) into (2.26), the closed-form expression of $|F_L^r(k_1)|^2$ is

$$|F_L^r(k_1)|^2 = \frac{\lambda_L^r}{\lambda_L^r + A_w}. \tag{2.27}$$

(iv) *Theoretical derivation of* $|F_L^r(k_1, k_2)|^2$. Substituting (C 3), (2.10) and (2.27) into (2.25), the closed-form expression of $|F_L^r(k_1, k_2)|^2$ is given by

$$|F_L^r(k_1, k_2)|^2 = \frac{(\lambda_L^r)^2}{(\lambda_L^r)^2 + k_2^2}. \tag{2.28}$$

By contrast, equation (2.28) has the same mathematical form as (B 2). Given $k_2 = 0$, equation (2.28) also satisfies the relation (2.22). This result validates the presented closed-form solution for admittances. Therefore, provided that the empirical coherence model of the lift is determined, the generalized one-wavenumber admittance and 3D AAF can be conveniently derived using the proposed procedure. It should be noted that the accuracy of the proposed approach mainly depends on the empirical coherence model. The approach proposed herein is still valid when the coherence model is replaced by others, e.g. Kimura's model.

2.3. *Effects of the decay parameters on the spanwise correlation of lift*

The spatial correlation of the lift on two different spanwise strips can be explored using the cross-correlation coefficient, which is given by

$$R_L(\Delta x, \Delta y) = \frac{\overline{L_1(x, y) L_2(x + \Delta x, y + \Delta y)}}{\tilde{L}_1 \tilde{L}_2}, \tag{2.29}$$

where L_1 and L_2 represent the lift at strips 1 and 2 respectively, the overbar denotes an ensemble average, $\Delta x = U\Delta t$ using Taylor's hypothesis, and Δy is the spanwise separation between two strips defined in figure 1. The quantities $\tilde{L}_1$ and $\tilde{L}_2$ are the standard deviations of $L_1(x, y)$ and $L_2(x + \Delta x, y + \Delta y)$, respectively. Generally, the size of the separation bubble plays an important role in determining the spatial correlation of the lift when the spanwise separation between two strips is not excessively large (Cherry, Hiller & Latour 1984; Kiya & Sasaki 1985). On the other hand, the effect of vortex shedding in separated flow should be emphasized instead of the large-scale vortices in the separation bubble when the separation is beyond the mean reattachment length, as the spatial correlation of the resulting smaller-scale vortices decreases rapidly as the spanwise separation increases. However, equation (2.29) can hardly account for this physical property, clearly because of the missing wavelength information of the vortices in the correlation coefficient due to the integration operation. By contrast, the spatial correlation defined by coherence allows us to clearly study the contribution of the vortices with different wavelengths.

In this section, the spanwise correlation of the lift is compared with that of the vertical velocity fluctuations to mathematically study the three-dimensional effects of turbulent flow, i.e. using the difference between the proposed coherence model for lift (2.13) and Jakobsen's model for the w component (see appendix C). In the following section, we take a two-step quantitative approach to this issue:

(i) *The sign of* Δ_{Coh}. Assuming that $A_w \neq \lambda_L$, the difference between the coherence of the lift force and w component, is defined as

$$\Delta_{Coh} = \mathrm{Coh}_L - \mathrm{Coh}_w. \tag{2.30}$$

By subtracting (C 1) from (2.9) (or (2.13)), we obtain

$$\Delta_{Coh} = \frac{A_w[\exp(-2\pi A_w \Delta y) - \exp(-2\pi \lambda_L \Delta y)]}{\lambda_L - A_w}. \tag{2.31}$$

The special case is to let $A_w \to \lambda_L$, whereby the limitation of (2.31) can be obtained by using L'Hopital's rule

$$\Delta_{Coh}|_{A_w \to \lambda_L} = 2\pi \lambda_L \Delta y \exp(-2\pi \lambda_L \Delta y). \tag{2.32}$$

The effects of three-dimensional turbulence depend on the sign of Δ_{Coh}, which is analysed based on the following three cases:

(1) Case 1: $0 < \Delta y < \infty$. Case 1 represents an aerofoil or rectangular cylinder with a finite span. In this case, the difference Δ_{Coh} in both (2.31) and (2.32) remains positive. This result indicates that the lift on line-like structures with a finite span is more strongly correlated than the vertical velocity fluctuations, due to the three-dimensional effects of turbulence. Thus, we mathematically interpret the phenomenon observed in previous wind tunnel tests, which may be an intrinsic property of the coherence of lift on an elongated body.

(2) Case 2: $\Delta y = 0$. Case 2 represents an aerofoil or rectangular cylinder with an infinitesimal span, which can be regarded as the two-dimensional cross-section of a body passing through transversely fully correlated turbulence (Fung 1969). In this case, the difference Δ_{Coh} becomes zero regardless of the decay parameters. This result implies that the spatial correlation of the gusts can be considered representative of that of the lift, which is essentially the strip assumption (Fung 1969).

(3) Case 3: $\Delta y = \infty$. Case 3 represents an aerofoil or rectangular cylinder with an infinite span. Thus, the solution to (2.31) can be easily obtained by calculating the limitation of Δ_{Coh} using L'Hopital's rule, which yields

$$\lim_{\Delta y \to \infty} \Delta_{Coh}|_{A_w \to \lambda_L} = \lim_{\Delta y \to \infty} \frac{1}{\exp(2\pi \lambda_L \Delta y)}. \tag{2.33}$$

When $\Delta y \to \infty$, both (2.32) and (2.33) become zero. This solution is reasonable, because the correlation of the lift or vertical velocity fluctuations vanishes when the spanwise separation is sufficiently large.

Similarly, it can be proved that the lift on an aerofoil or rectangular cylinder is more strongly correlated than the 3D AAF defined by (B 6) based on the above-mentioned procedure. Massaro & Graham (2015) studied the spanwise correlation of lift numerically by defining of the correlation length scale, and similar results were obtained. In contrast, it should be noted that a larger correlation length scale does not suggest that the spanwise correlation is also larger for arbitrary wavenumber k according to Bracewell's approach (Bracewell 1978). This issue is further discussed from the experimental perspective in § 3.2.

(ii) *The monotonic behaviour of* Δ_{Coh}. In step (i), the sign of Δ_{Coh} is analysed, and the effects of the decay parameters must be further studied with respect to case 1, i.e. the finite span section ($0 < \Delta y < \infty$). According to the proposed coherence model (2.9) or (2.13), it should be noted that the decay parameters λ_L and A_w, associated with the 3D AAF and w component, respectively, primarily determine the coherence of the lift. Thus, the difference Δ_{Coh} defined by (2.31) is applied to analyse the effects of the decay parameters on the spanwise correlation of the lift force. By defining $\lambda_L = A_w + \delta$ ($\delta \in [-\infty, \infty]$), equation (2.31) can be rewritten as

$$\Delta_{Coh} = \mathrm{Coh}_L - \mathrm{Coh}_w = \frac{\varepsilon[1 - \exp(-2\pi\delta\Delta y)]}{\delta}, \tag{2.34}$$

with

$$\varepsilon = A_w \exp(-2\pi A_w \Delta y), \tag{2.35}$$

where ε is a positive function associated with A_w and Δy. Therefore, the effects of the decay parameters are simply attributed to the monotonicity of $\Delta_{Coh}(\delta)$. By using the derivation method, we have

$$\frac{\mathrm{d}\Delta_{Coh}}{\mathrm{d}\delta} = \frac{\varepsilon[1 - \exp(-2\pi\delta\Delta y)(1 + 2\pi\delta\Delta y)]}{-\delta^2}. \tag{2.36}$$

When $\delta \to 0$, the solution of (2.36) can be obtained by determining its limit according to L'Hopital's rule, giving

$$\begin{aligned} \lim_{\delta \to 0} \frac{\mathrm{d}\Delta_{Coh}}{\mathrm{d}\delta} &= \lim_{\delta \to 0} \frac{\varepsilon(2\pi\Delta y)^2 \delta \exp(-2\pi\delta\Delta y)}{-2\delta} \\ &= \lim_{\delta \to 0} \frac{\varepsilon(2\pi\Delta y)^2[(1 - 2\pi\delta\Delta y)\exp(-2\pi\delta\Delta y)]}{-2} \\ &= \frac{\varepsilon(2\pi\Delta y)^2}{-2}. \end{aligned} \tag{2.37}$$

Integral length scale		Intensity	
L_u^x (m)	L_w^x (m)	I_u (%)	I_w (%)
0.107	0.054	8.0	6.5

TABLE 1. Characteristics of grid-generated turbulence based on least-squares fit of the von Kármán spectrum.

In this case, the above-mentioned limit remains negative, which means that $\Delta_{Coh}(\delta)$ is monotonically decreasing, i.e. the smaller δ is, the larger the spanwise correlation of the lift becomes relative to that of w.

When $\delta \neq 0$, the monotonic behaviour of $\Delta_{Coh}(\delta)$ depends on the sign of the numerator in (2.36), defined by

$$\phi = \varepsilon[1 - \exp(-2\pi\delta\Delta y)(1 + 2\pi\delta\Delta y)]. \tag{2.38}$$

Thus, the derivative of ϕ is given by

$$\frac{\mathrm{d}\phi}{\mathrm{d}\delta} = \varepsilon(2\pi\Delta y)^2\delta\exp(-2\pi\delta\Delta y), \tag{2.39}$$

which approaches zero when $\delta \to 0$. It is clear that the sign of (2.39) depends only on δ. When $\delta < 0$, equation (2.39) is negative, and thus (2.36) is monotonically increasing, and *vice versa*. This result implies that the three-dimensional effects of turbulence become more prominent as δ decreases over the entire frequency domain. Hence, using mathematical treatment, the effects of cross-sectional shape and three-dimensional flow on the spanwise correlation of the lift can be interpreted quantitatively in a clearer manner.

With respect to a given gust field, the above-mentioned analysis provides explicit insight into the physical phenomenon in which the lift on an aerofoil or other line-like structure becomes more strongly correlated with the increasing correlation of the 3D AAF. In addition, this enhancement depends on the difference δ between λ_L and A_w. This theoretical derivation can be verified by the experimental investigation in the next section using three sectional models with different cross-sectional shapes.

3. Experimental investigation

Experiments were conducted in a wind tunnel with a 2.4 m (width) $\times$ 2 m (height) working section (XNJD-1 wind tunnel). The tunnel is of the closed-circuit type and has a free-stream turbulence level of approximately 0.3 % and a top speed of 45 m s^{-1}. A highly turbulent flow was generated by the installation of a uniform grid 4.2 m upstream of the model in the streamwise direction. The grid was constructed of bars of rectangular cross-section with a mesh size of 0.33 m $\times$ 0.33 m and a bar size of 0.07 m. The turbulence parameters in three directions, shown in table 1, were measured simultaneously using Series 100 Cobra Probe, and the angle of attack of the incoming flow was zero in the experimental investigation.

To validate the presented spectral and coherence model, three sectional models were used. The model, with a NACA 0015 cross-section, was mounted normal to the flow to assess the validity of the double-exponent coherence model (2.9). The model was made of fibreglass, with several ribs to increase its stiffness and a chord length is

0.5 m. The 0.7 m long centre portion (action model) of the model was instrumented to measure the unsteady surface pressures on six strips along the span. Two 0.4 m long pseudomodels and end plates were installed at each end of the action model to ensure the two-dimensionality of the flow and to reduce end effects. Similarly, the other two models, with rectangular cross-sections of 0.2 m $\times$ 0.1 m (aspect ratio: $B/D = 2:1$) and 0.4 m $\times$ 0.1 m (aspect ratio: $B/D = 4:1$), were mainly used to investigate the effects of the decay parameters, λ_L^r and A_w, on the spatial distribution of the lift force and the distortion of the free stream when turbulent flow passed through the models. It should be noted that the lengths of the two rectangular models, including the centre portions and pseudomodels, were consistent with those of the NACA 0015 model.

The dynamic force measurements were based on simultaneous measurements of surface pressures around six chordwise strips in the centre portion of the three models. The pressure distribution of each strip was measured using 50 pressure taps for the $B/D = 2:1$ model and 60 pressure taps for the other two models. Six DMS 3400 pressure transducers were used to synchronously measure surface pressure fluctuations on those models. The transducers were mounted directly inside the models and connected to pressure tapings with PVC tubing with an internal diameter of 1.5 mm. Thus, the tube length could be kept to a minimum (0.2 m), ensuring a good frequency response up to 256 Hz. By integrating the surface pressures, the time-varying lift on each strip could be obtained for later spectral and coherence analyses. The contribution of skin-friction to the lift on the motionless models was not taken into account, because the angle of attack was zero and the surface was well polished to keep the roughness of those models low.

To facilitate the calculation of the 3D AAF, the sampling frequency of the Cobra Probe and pressure scanners was set to 256 Hz. The low-frequency eddies that carry most of the energy in turbulence were of primary interest (see figure 2). Therefore, the sampling rate used herein was sufficient to capture the major turbulence spectrum. Wind tunnel tests were typically conducted at a mean wind speed of 11.5 m s^{-1} with the Reynolds number Re ranging from 5.7×10^4 to 7.7×10^4, where $Re = UD/\upsilon$, D is the height of the model, and υ is the kinematic viscosity.

3.1. *The characteristics of grid-generated turbulence*

In wind tunnels, homogeneous turbulence can be approximately simulated by a square-mesh grid (Batchelor 1959). Models based on the von Kármán spectrum can be applied in the present work, because they can describe grid-generated turbulence well (Roberts & Surry 1973; Larose & Mann 1998; Li *et al.* 2015). The one- and two-wavenumber spectra of the vertical velocity fluctuations proposed by Taylor (1965) are described by

$$S_w(k_1) = \frac{2\sigma_w^2 L_u^x [1 + (8/3)(2\pi a k_1)^2]}{[1 + (2\pi a k_1)]^{11/6}}, \tag{3.1}$$

$$S_w(k_1, k_2) = \frac{(128/9)\sigma_w^2 \pi^3 a^4 (k_1^2 + k_2^2)}{[1 + 4\pi^2 a^2 (k_1^2 + k_2^2)]^{7/3}}, \tag{3.2}$$

with the parameter a given by

$$a = L_u^x [\sqrt{\pi}\Gamma(\beta + \tfrac{1}{2})/\Gamma(\beta)]^{-1}, \tag{3.3}$$

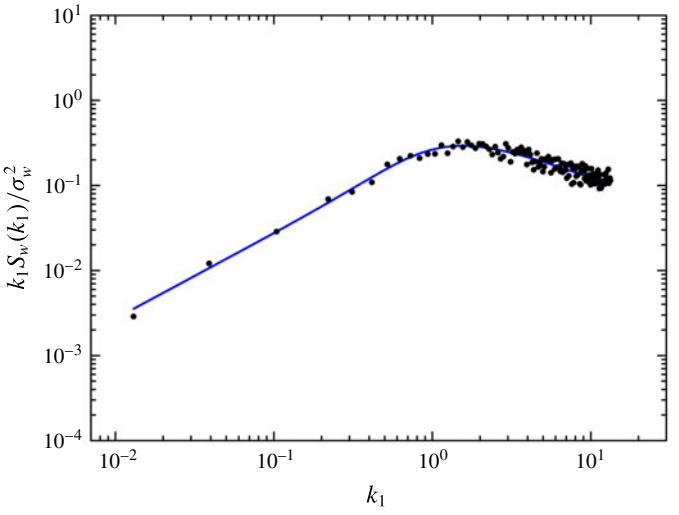

FIGURE 2. (Colour online) Spectrum of the vertical wind fluctuations for grid turbulence (●). Solid line: fit of von Kármán spectrum using (3.1) with $\beta = 1/3$.

where $\beta = 1/3$, L_u^x is the longitudinal integral length scale of turbulence with $L_u^x = 2L_w^x = 2L_v^x$ for homogeneous isotropic turbulence, $\Gamma(\beta)$ is the Gamma function, and σ_w is the root mean square (r.m.s.) of vertical velocity fluctuations.

To characterize the flow condition in the section model position, the one-wavenumber spectrum of the w component is compared with the theoretical result (3.1) in figure 2. It is observed that the measured result corresponds particularly well with (3.1) as $\beta = 1/3$, as proposed by Taylor (1965), suggesting that the grid-generated flow field satisfies the assumption of homogeneity and isotropy. Moreover, the measured results confirm that the indirectly measured two-wavenumber spectrum of w (3.2) is of high accuracy (Li *et al.* 2015). Table 1 presents the fitted results and summarizes the characteristics of the turbulence. Specifically, the integral length scales are obtained by fitting with the experimental spectrum using the von Kármán model (3.1). The result shows that L_u^x is nearly double L_w^x, which is consistent with the property of homogeneous isotropic turbulence. However, the property of isotropic turbulence that suggests that the variances σ_u^2 and σ_w^2 must be equal is not supported by data (Mann 1994), including those obtained from the present experiments, which depend on the averaging time (usually approximately 10 min for meteorological measurements) and the effects of anisotropic component in the flow (Mann 1994; Larose 1997).

The coherence of homogeneous isotropic turbulence can be calculated analytically in terms of Bessel functions for the von Kármán spectrum (Irwin 1977). However, such a model is somewhat complex when used to analyse the effect of three-dimensional turbulence on the buffeting lift force. Instead, Jakobsen's empirical model is adopted to provide the decay parameter A_w for the proposed coherence models (2.9) and (2.13). Thus, the accuracy of Jakobsen's model is assessed in figure 3 by comparison with the experimental results. The three parameters in A_w can be determined using the nonlinear least-squares fit method and are presented in table 2.

It is clear that Jakobsen's empirical coherence model generally agrees with the measured results, thus providing an accurate estimate of the decay parameter A_w for the proposed coherence model.

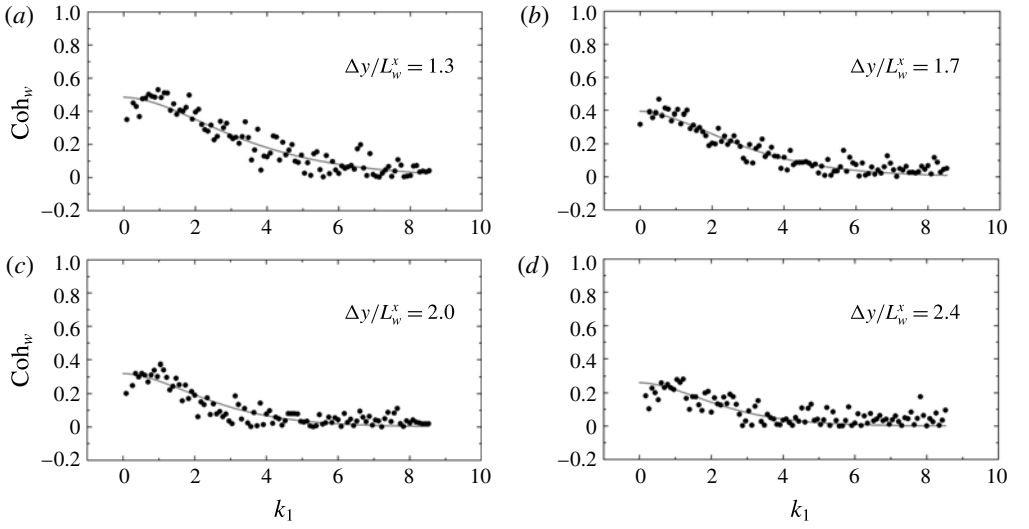

FIGURE 3. Coherence of vertical velocity fluctuations in grid-generated turbulence (●). Solid line: fit of Jakobsen's empirical model using (C 1) and (C 2).

Cross-section		Floating parameters					
		A_w			λ_L		
		c_1	c_2	c_3	a_1	a_2	a_3
NACA 0015	Measured result	1.1619	0.6049	5.1266	0.0796	1.7383	0.3994
	Mugridge's model	1.1619	0.6049	5.1266	1.0000	2.0000	0.1013
	Blake's model	1.1619	0.6049	5.1266	0.4714	0.5000	0.1042
Rectangular cylinder	$B/D = 2:1$	1.1619	0.6049	5.1266	0.6162	2.3057	0.0503
	$B/D = 4:1$	1.1619	0.6049	5.1266	0.4400	2.4135	0.3196

TABLE 2. Parameters of the double-exponent coherence models fitted by the measured results.

3.2. *The spatial distribution of lift force on rectangular cylinders*

3.2.1. *Validation of the proposed coherence model*

To validate the proposed coherence model in § 2, an experimental investigation of the NACA 0015 model is performed. The lift forces on the chordwise strips were obtained based on simultaneous measurements of surface pressures. The proposed coherence model is compared with the measured results in figure 4, and the parameters in λ_L are presented in table 2, obtained using the least-squares fit method. The results of the proposed coherence model agree well with the measurements when $\Delta y/L_w^x < 6$, although the model's accuracy decreases slightly at very low frequency when the dimensionless separation $\Delta y/L_w^x$ increases. The experimental results thereby confirm that the proposed coherence model is of sufficiently high accuracy, which ensures the reliability of the following parameter analysis.

The proposed coherence model can be further validated by comparison with Mugridge's and Blake's theoretical results. In our previous paper (Li *et al.* 2015), we confirmed that Mugridge's 3D AAF is only of high accuracy at low frequency ($k_1 < 1/\pi$) and that Blake's approximate expression is more accurate when the

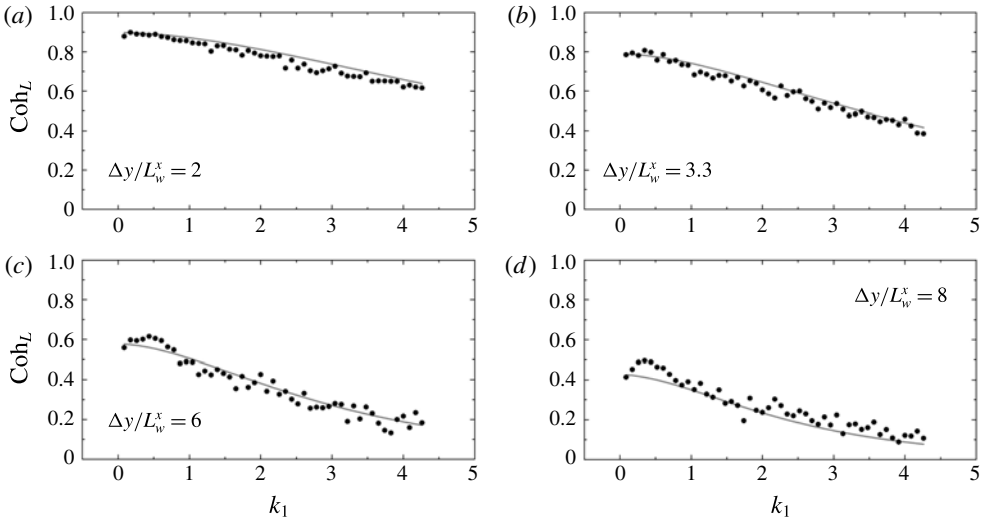

FIGURE 4. Comparisons of the coherence of lift on NACA 0015 between the proposed coherence model (solid line) and experimental results (●).

reduced frequency is not particularly low. For verification, this conclusion is further investigated in this study by comparing the predicted correlation coefficients of lift with the experimental results. Using the proposed coherence model, the correlation coefficient can be numerically calculated as follows:

$$R_L(\Delta y) = \frac{\displaystyle\int_0^\infty S_L(k_1, \Delta y)\,\mathrm{d}k_1}{\displaystyle\sqrt{\int_0^\infty S_L(k_1, y_1)\,\mathrm{d}k_1 \int_0^\infty S_L(k_1, y_2)\,\mathrm{d}k_1}}. \tag{3.4}$$

Then, by substituting (2.3)–(2.7) into (3.4) and using the parameters provided in table 2, the correlation coefficients of the lift on aerofoil can be determined as shown in figure 5.

The calculated results using Mugridge's parameters can hardly describe the spanwise correlation of the lift force on a thin aerofoil relative to the laboratory measurements, particularly for the cases with a large spanwise separation. In contrast, Blake's results, as well as those obtained using the proposed coherence model, are in agreement with the experimental measurements. Similar results were obtained in our preceding studies (Li *et al.* 2015). Therefore, it is worth mentioning that the proposed coherence model, based on Ribner's three-dimensional theory, is valid for the lift on a thin aerofoil.

3.2.2. *The application of the proposed coherence model to rectangular cylinders*

In this section, the application of the proposed coherence model (2.13) to rectangular cylinders is investigated. The proposed coherence model is compared in figures 6 and 7 with the results measured for rectangular cylinders with aspect ratio $B/D = 2$ and $B/D = 4$, respectively. Using least-squares fit method, the three floating parameters in λ_L^r were obtained as shown in table 2.

As shown in figure 6, the proposed coherence model agrees well with the experimental measurements, except at rather low frequency or in the vortex-shedding

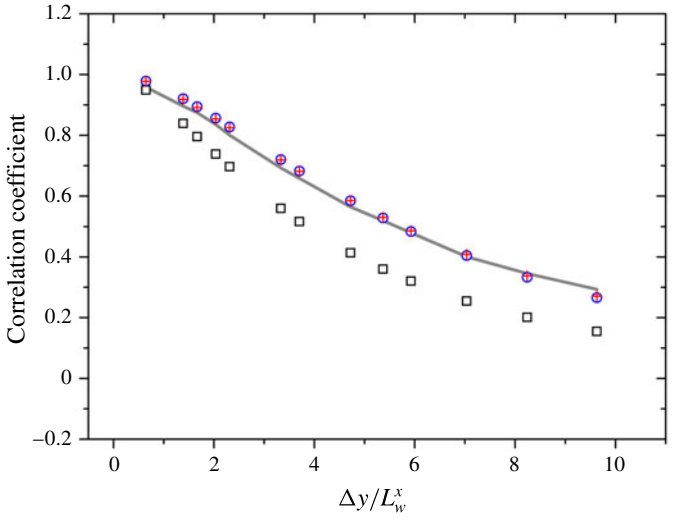

FIGURE 5. (Colour online) Comparisons between the experimentally measured correlation coefficient of the lift force on NACA 0015 (solid line) and the theoretical calculations based on the double-exponent coherence model: (□), Mugridge's decay parameter (B 3); (○), Blake's decay parameter (B 4); (+), empirical decay parameter (2.14).

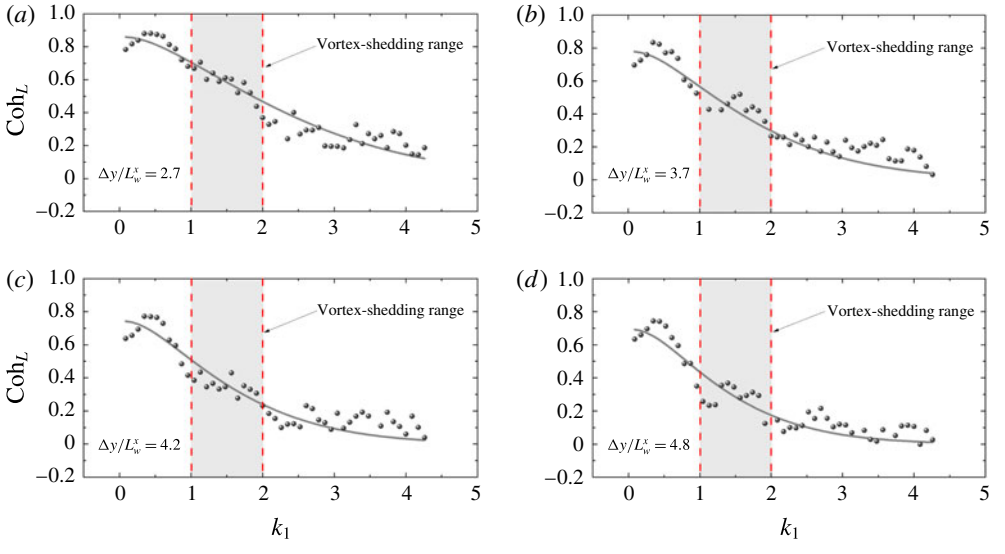

FIGURE 6. (Colour online) Comparisons between direct measurements of the spanwise coherence of the lift force on a rectangular cylinder with an aspect ratio of $B/D = 2$ (●) and the proposed coherence model (solid line).

range. In addition, it is noted that the peak in the vortex-shedding range can increase to up to 0.58, which may be related to the Strouhal number, aspect ratio and flow characteristics, such as turbulence intensity, the integral length scale and the fluid viscosity. Similar results are shown in figure 7 with respect to the rectangular cylinder with $B/D = 4$. However, the effects of the deviation between the proposed coherence

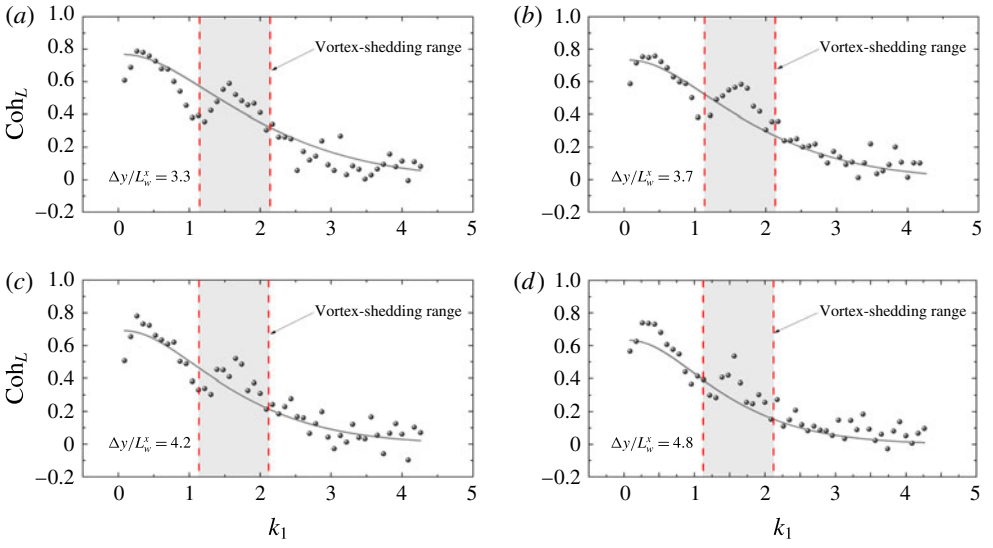

FIGURE 7. (Colour online) Comparisons between direct measurements of the spanwise coherence of the lift force on a rectangular cylinder with an aspect ratio of $B/D = 4$ (●) and the proposed coherence model (solid line).

model and the experimental results in the low-frequency domain and vortex-shedding frequency range on the one-point spectrum of lift on the sectional strip are negligible. Therefore, the proposed coherence model is of acceptable accuracy for rectangular cylinders, although it is apparently not the most optimized option; that option would provide better insight into the coherence of lift and the effects of parameters λ_L and A_w.

3.2.3. *The optimum option for describing the spanwise correlation of lift*

It is clear that the lift fluctuations on a thin aerofoil are directly related to the vertical velocity fluctuations in the free stream when the flow remains attached. In contrast, the lift fluctuations on a bluff body are mainly determined by the characteristics of flow separation and reattachment. Hence, it is expected that the size of the separation bubble has an important effect on the spanwise correlation of the lift fluctuations (Cherry *et al.* 1984; Sankaran & Jancauskas 1993). It should be noted that (2.13)–(2.14) provide a simplified model accounting for the effects of three-dimensional turbulence on the spanwise correlation of lift on bluff bodies. The correlation coefficient, correlation length scales and correlation width are also usually applied to describe the spanwise correlation of the lift force. The first two are defined by (2.8) and (3.4), respectively, and the correlation length scale defined by Massaro & Graham (2015) is a function of the wavenumber obtained by integrating the coherence of turbulence and lift as follows:

$$L^y(k_1) = \int_0^\infty \mathrm{Coh}_{12}(k_1, \Delta y)\, \mathrm{d}\Delta y, \tag{3.5}$$

where $\mathrm{Coh}_{12}(k_1, \Delta y)$ is the coherence defined by (2.8). The correlation width defined by Larose & Mann (1998) is expressed by integrating the correlation coefficients,

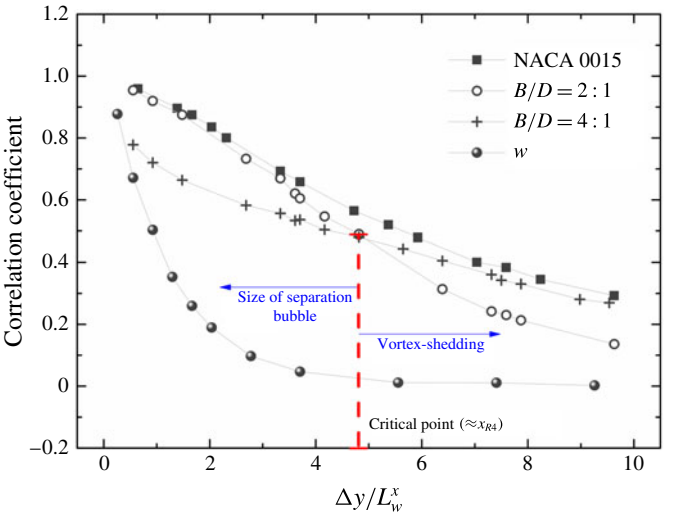

FIGURE 8. (Colour online) Correlation coefficients of lift forces and vertical velocity fluctuations behind the uniform grid.

which yields

$$L^y = \int_0^\infty R_{12}(\Delta y)\,\mathrm{d}\Delta y, \tag{3.6}$$

where $R_{12}(\Delta y)$ is the correlation coefficient.

In figure 8, the spanwise correlation coefficients of vertical velocity fluctuations behind a uniform grid are compared with those of the lift forces on three sectional models. The results show that the spanwise correlation of lift forces is greater than that of the w component, which is well consistent with the results reported in previous studies. Interestingly, the spanwise correlation of lift on a thin aerofoil is greater than that on rectangular cylinders, which should be attributed to the attachment of the flow. With respect to the rectangular cylinders, the spanwise correlation of the lift force on the $B/D = 2$ section is greater than that on the $B/D = 4$ section when $\Delta y/L_w^x$ is less than 4.8 ($\approx x_{R4}/L_w^x$ or 1.6 x_{R2}/L_w^x, where x_{R4} and x_{R2} are the mean reattachment lengths of the rectangular models with $B/D = 4$ and 2, respectively), and *vice versa*. The experimental results verify that the spanwise correlation of lift is related to the aspect ratio and separation between two strips (Larose & Mann 1998; Ito *et al.* 2014). The phenomenon illustrated in figure 8 can be interpreted by the physical characteristics of flow separation and reattachment. As the aspect ratio decreases, the size of the separation bubble is reduced in length and height (i.e. $B/D = 2$), which, in turn, reduces the pressure fluctuations within the separation bubble. Consequently, the vortices of the rectangular section become more two dimensional, resulting in a larger spanwise correlation of lift on the model with $B/D = 4$, while the spanwise separation Δy is smaller than x_{R4}. When $\Delta y > x_{R4}$, the opposite tendency of the spanwise correlation of lift is likely caused by the preceding vortex shedding from the reattachment point of the $B/D = 2$ section ($x_{R2} \approx 0.6x_{R4}$) and the resulting small-vortex structures (more 3D). However, the correlation coefficient clearly fails to demonstrate the spanwise correlation of vortices of various wavelengths.

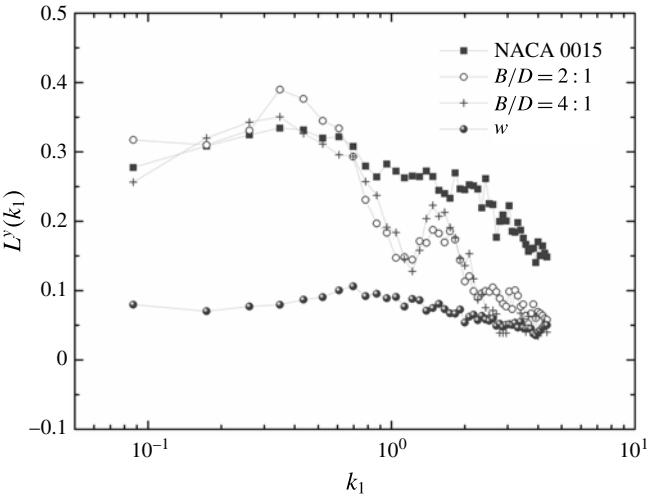

FIGURE 9. The correlation length scales of lift forces and vertical velocity fluctuations defined by (3.5) using experimental measurements of coherence in wind tunnel tests.

Type	Lift force			Vertical velocity fluctuations
	NACA 0015	$B/D = 2:1$	$B/D = 4:1$	
Correlation width (m)	0.2767	0.2456	0.2422	0.054

TABLE 3. Correlation widths of vertical velocity fluctuations and lift forces.

Using (3.5) and the experimental measurements of coherence presented in figures 3, 4, 6 and 7, the correlation length scales of the lift and the w component can be obtained as shown in figure 9. It should be noted that the correlation length scales of lift are greater than those of the w component. Compared with the correlation coefficient, this representation can clearly reflect the effects of vortex shedding on the spanwise correlation of the lift on rectangular cylinders as shown in figure 8. However, the model masks information regarding the variations of the spanwise correlation of the lift with the separation between two strips along the span of the rectangular cylinders.

Using (3.6), the correlation widths of the lift and the w component can be obtained from figure 8, and the results are presented in table 3. Apparently, the correlation widths of the lift force on elongated bodies, including the aerofoil and rectangular cylinders examined herein, are much larger than those of the w component. The results are in agreement with the above-mentioned studies. However, it is observed that the correlation width of lift on the aerofoil is similar to the correlation widths on the rectangular cylinders. Compared with the results obtained using the three evaluation methodologies, the correlation width contains much less information regarding the effects of spanwise separation, aspect ratio and cross-sectional shape because of the integration over wavenumber and spanwise separation.

Consequently, it can be concluded that the correlation coefficient, correlation width and correlation length scales are not the optimal option for describing the spatial correlation of two random variables compared with coherence, as they are

not mathematically rigorous in describing the spatial correlation of lift varying with wavenumber and separation as discussed in § 2.3. In the next section, coherence is applied to study the effects of the decay parameters on the spanwise correlation of the lift on elongated bodies by wind tunnel tests.

3.2.4. *The effects of decay parameters*

It should be noted that the fitted results in table 2 are obtained using the total nonlinear least-squares method, which would partially mask the information regarding the variations of the spanwise correlation of lift with dimensionless separations. Therefore, taking three specific separations for instance, i.e. $\Delta y/L_w^x = 3.3$, 4.8 (mean reattachment length x_{R4}, see figure 8) and 7.6, the decay parameters in the proposed coherence model are fitted by the nonlinear least-squares approach separately to further study the phenomenon illustrated in figure 8. For the sake of readability, we use the names in the legend of figure 10 to represent the corresponding decay parameters and coherence hereafter.

When $\Delta y/L_w^x = 3.3$, figure 10(*a*) shows that the decay parameters λ_L are smaller than A_w when k_1 is within 0.5 (defined as critical point of wavenumber), i.e. $(B/D = 2:1) < (\text{NACA } 0015) < (B/D = 4:1) < (w)$. As discussed in § 2.3, the three-dimensional effects of the turbulence become more prominent as the difference between λ_L and A_w decreases. In other word, the coherence of the lift forces on bodies should have the opposite tendency of the decay parameters, i.e. $(w) < (B/D = 4:1) < (\text{NACA } 0015) < (B/D = 2:1)$, which is consistent with the results shown in figure 10(*b*). With respect to the other two separations, figure 10(*c–f*) can further validate the theoretical analysis conducted in § 2.3.

Interestingly, it appears that the critical wavenumber is kept approximately constant regardless of the cross-sectional shape and spanwise separation, dependent only on the turbulent flow field. Moreover, the results suggest that the smaller-scale vortices ($k_1 > 0.5$) stretch more greatly along the span of the aerofoil than those passing through the rectangular cylinders. This finding may be attributed to the attached flow mentioned previously.

Compared with that of the $B/D = 4$ section, figure 10(*a*,*b*) suggests that the contribution of the larger-scale vortices to the spanwise correlation of the lift on the model with a smaller aspect ratio is more distinct because the separation bubble decreases in length but becomes more elongated in the spanwise direction (more 2D). In particular, when $\Delta y/L_w^x = 4.8$, as shown in 10(*c*,*d*), the vortices around two strips on the rectangular cylinders with different aspect ratios may have similar spatial characteristics, including their length scale and phase, which are highly complex and should be further studied using the flow field visualization method. When $\Delta y/L_w^x > 4.8$, the spatial correlation of the lift forces on rectangular cylinders is primarily dominated by the resulting small eddies in the body-induced vortices. In this case, these small-scale vortices stretch more rapidly spanwise than they do chordwise during eddy formation and shedding. Consequently, the three-dimensionality of the vortex shedding and the 2D character of the separation bubbles can partly explain the larger contribution of high-frequency vortices, as shown in figure 10(*e*,*f*). Therefore, the effect of the aspect ratio on the spanwise correlation of the lift on rectangular cylinders is significant and should be more closely examined (Bearman 1971, 1972; Kiya & Sasaki 1983, 1985; Cherry *et al.* 1984; Nakamura & Ozono 1987).

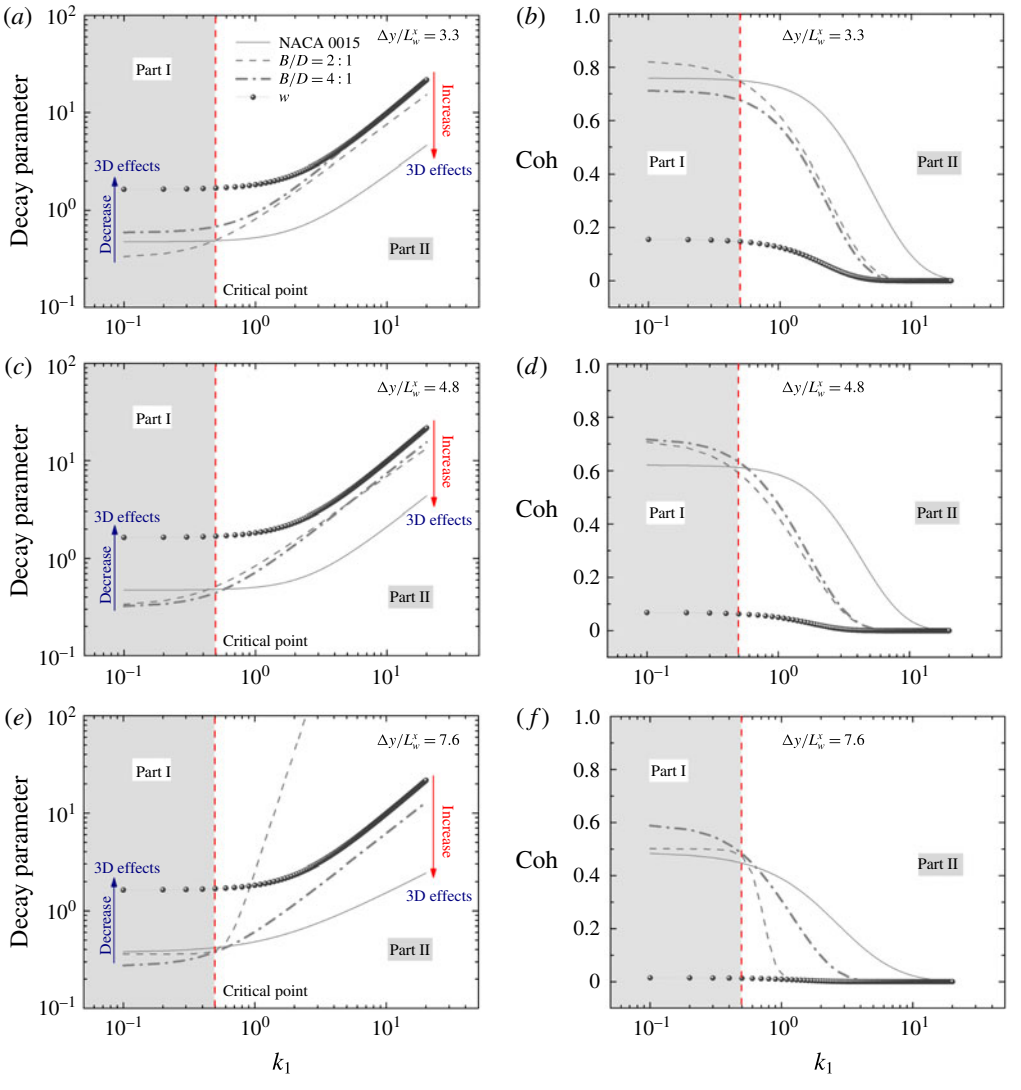

FIGURE 10. (Colour online) The relationship between the decay parameters (λ_L and A_w) and the coherence of the lift on experimental models with different cross-sectional shapes.

3.2.5. *The energy transition*

In this section, the energy transition is discussed using the proposed 3D AAF model in the two-wavenumber domain, which allows us to understand the phenomenon by which the lift on a rectangular cylinder is more strongly correlated than the vertical velocity fluctuations in the free stream.

Previous studies (Bearman 1971, 1972) have indicated that the vortex line filaments would be stretched and rotated when turbulence approaches a body, which is of interest in studying the spanwise correlation of the lift on bluff bodies. With respect to the aerofoils, Li *et al.* (2015) investigated this distortion problem from the perspective of the energy transition, conducting two-wavenumber spectral analyses of velocity and lift as well as of aerodynamic admittance and coherence. Similarly, this approach

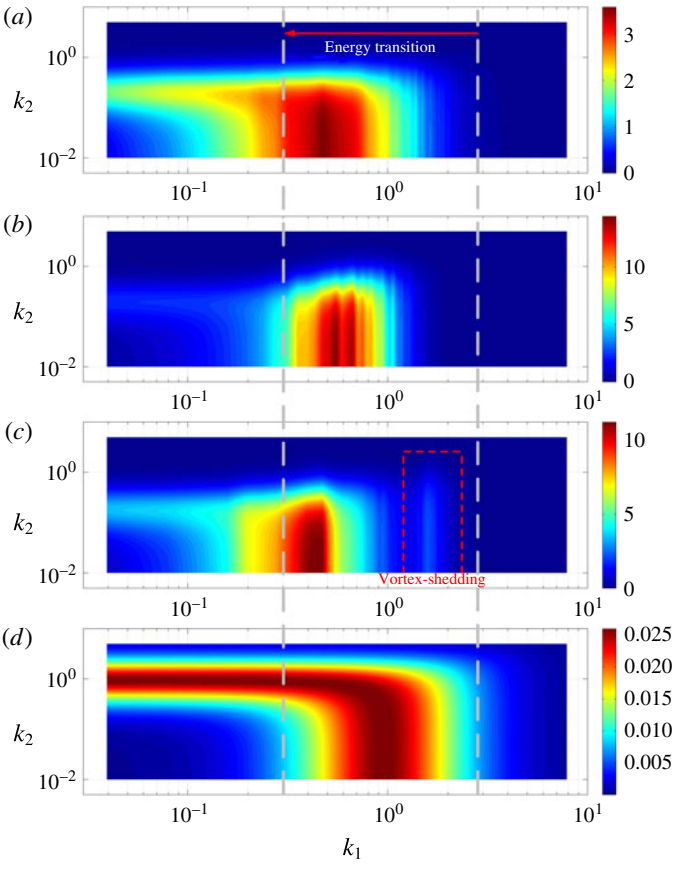

FIGURE 11. Contours of two-wavenumber spectra of lift forces and vertical velocity fluctuations. (*a*) Lift force on NACA 0015 model. (*b*) Lift force on rectangular cylinder with $B/D = 2:1$. (*c*) Lift force on rectangular cylinder with $B/D = 4:1$. (*d*) Vertical velocity fluctuations.

is implemented with respect to the rectangular cylinder examined in the present work. The two-wavenumber spectra of the lift forces can be obtained by substituting (2.28) and (3.2) into (2.19). The results are shown in figure 11.

The wavenumber associated with the peak of $S_L(k_1, k_2)$ in the spanwise direction is lower than that of the vertical velocity fluctuations. It is clear that the energy of the lift forces on the bodies is transferred to larger-scale vortices in both the chordwise and spanwise directions. This phenomenon indicates that the vortex stretching in the spanwise direction results in a larger correlation of lift on bodies from an energetic perspective. Compared with that on the rectangular cylinders, the stronger spanwise correlation of the lift on the aerofoil may be induced by a larger proportion of vortex energy in the spanwise direction. With respect to the chordwise direction, the wavenumber of the rectangular cylinder related to the peak of $S_L(k_1, k_2)$ is lower than that of NACA 0015 and decreases as the aspect ratio increases. In addition, the higher the aspect ratio of the rectangular cylinder is, the more remarkable the effects of the vortex shedding on the spatial correlation of the lift force become.

Using (2.28), the 3D AAF of the three models can be obtained as shown in figure 12. Generally, the admittance can be regarded as a low-pass filter that transfers

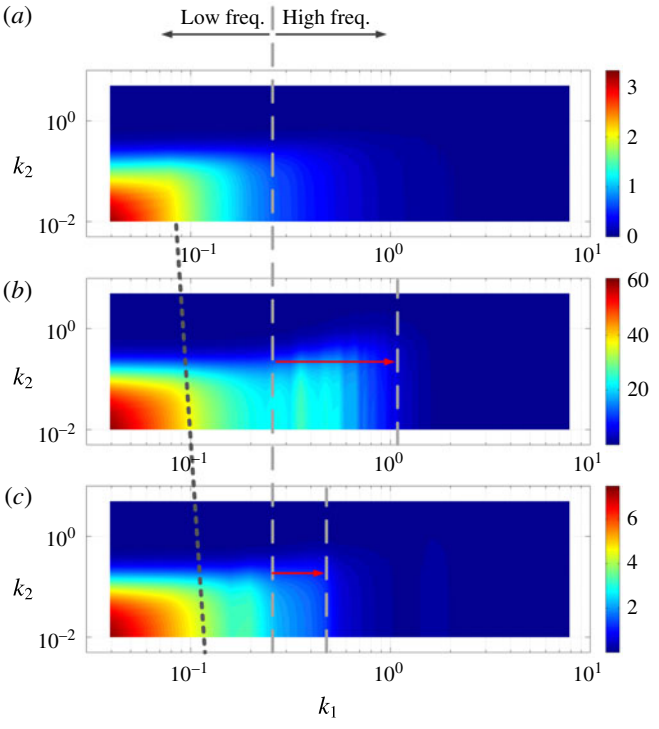

FIGURE 12. Contours of 3D AAF on an aerofoil and rectangular cylinders. (*a*) NACA 0015 model. (*b*) Rectangular cylinder with $B/D = 2:1$. (*c*) Rectangular cylinder with $B/D = 4:1$.

energy from high to low frequency (Li *et al.* 2015). In the low-frequency range, the filtered bandwidths have the following relations: (NACA 0015) $<$ $(B/D = 2:1)$ $<$ $(B/D = 4:1)$. The results suggest that larger-scale vortices are contaminated by smaller eddies such that the entrainment rate is increased. Consequently, the spanwise correlation of the lift should have the opposite tendency, which can be confirmed by the coherence results presented in figure 10, where k_1 is within the range of critical wavenumbers. Regarding the high-frequency range, the contributions of small-scale vortices on the rectangular cylinder with $B/D = 2:1$ are clearly greater than those on the other two models. Thus, the results provide insight, from an energetic perspective, into the smaller correlation of lift shown in figure 10(*f*).

To further investigate the spanwise correlation of the lift from an energy point of view, the two-wavenumber coherence of the lift forces and vertical velocity fluctuations are obtained as shown in figure 13. In contrast with the two-wavenumber spectra demonstrated in figure 11, the two-wavenumber coherence can more directly describe the relationship between the spatial correlation of the lift and the energy-transition process. In the spanwise direction, the results coincide strongly with those obtained from the two-wavenumber spectra (see figure 11), providing the evidence of extended spanwise structures of vortices with spanwise coalescence (Cherry *et al.* 1984). Regarding the chordwise direction, it is observed that the peak energy is transferred to a lower frequency from the NACA 0015 model to the $B/D = 4$ one, which indicates that vortex stretching occurs in the streamwise direction when the turbulent flow passes through the bodies. Nevertheless, it should be noted that the

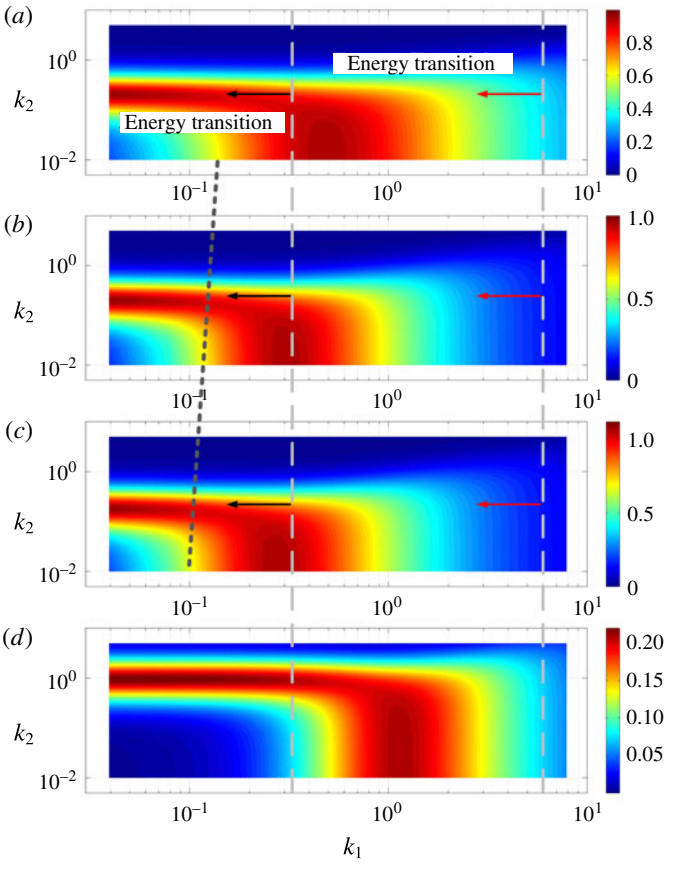

FIGURE 13. Contours of two-wavenumber coherence of lift forces and vertical velocity fluctuations. (*a*) $\Phi_L(k_1, k_2)$ of NACA 0015 model. (*b*) $\Phi_L(k_1, k_2)$ of rectangular cylinder with $B/D = 2:1$. (*c*) $\Phi_L(k_1, k_2)$ of rectangular cylinder with $B/D = 4:1$. (*d*) $\Phi_w(k_1, k_2)$ of vertical velocity fluctuations.

effect of vortex shedding on the spanwise correlation of the lift on the rectangular cylinders can hardly be described by using the proposed coherence model. Further improvement is required for the proposed model to quantitatively explain this effect.

4. Conclusion

Using Ribner's three-dimensional spectral tensor theory and the inverse Fourier transform, a double-exponential coherence model is proposed to study the effects of three-dimensional turbulence and 3D AAF on the spanwise correlation of the lift force on aerofoils and rectangular cylinders. Based on this model, we find that the spanwise correlation of lift on line-like structures is intrinsically greater than that of the oncoming flow and 3D AAF. The presented model can be implemented in line-like structures of complex cross-sections because of the definitions of floating parameters. However, it is difficult to obtain the analytical solutions of these parameters, which must be determined by wind tunnel tests. Moreover, a generalized approach is proposed to derive the closed-form expression of the 3D AAF according to the

coherence model of the lift. Hence, the problem of 3D AAF becomes an issue of experimentally determining a more accurate coherence model of lift.

According to the experimental investigation, it is observed that the proposed coherence model becomes more accurate as the shape of the cross-section approaches that of a thin flat plate. The discrepancy observed for the proposed coherence model in the vortex-shedding range can be neglected from the viewpoint of analysing the buffeting response analysis, because the frequency of vortex shedding is much higher than the natural frequency of the structures. Using this model, the effects of the decay parameters associated with the 3D AAF and w component can be studied mathematically. The three-dimensional effect of turbulence becomes more prominent as the difference between λ_L and A_w decreases, which is also experimentally validated herein. Furthermore, the experimental investigation suggests that the spanwise correlation of the lift on bodies is related not only to the scale of eddies but also to the spanwise separation between two strips. Therefore, coherence is the most appropriate means of describing the spatial correlation of the lift. The experimental results also demonstrate that the spanwise correlation of the lift on the aerofoil is more strongly correlated than that on the rectangular cylinders because of the attachment of flow. It is worth noting that the effect of the aspect ratio on the spanwise correlation of the lift forces on the rectangular cylinders is primarily attributed to the size of the separation bubble and smaller eddies in the vortex-shedding range.

Based on two-wavenumber spectral analysis, the spatial correlation of the lift on rectangular cylinders is investigated from an energy-transition perspective. It can be observed that the energy is transferred from high frequency to low frequency in a similar manner to that of the aerofoil. In addition, if the effect of vortex shedding on the spatial distribution of the lift force on a rectangular cylinder is more closely examined, the proposed coherence model should be further improved.

Acknowledgements

This work is supported by the National Natural Science Foundation under grant nos 51608074, 51478402, 51578098 and the Fundamental Research Funds for the Central Universities with project no. 106112017CDJQJ208849. We are indebted to Professor Tamura (Tokyo Polytechnic University, Japan), Dr N. Yeung (ARUP, HongKong) and Ms Smarika (Goldwind Science & Technology, Beijing) for their valuable comments and suggestions, which greatly enhanced the quality of this article.

Appendix A

A.1. *Spectral model of homogeneous turbulence*

In this section, we discuss the statistical and spectral characteristics of homogeneous turbulence. Suppose we measure turbulent velocity fluctuations at two points in space, $\boldsymbol{x}_1 = (x_1, y_1, z_1)$ and $\boldsymbol{x}_2 = (x_2, y_2, z_2)$, with the coordinate system defined as in figure 1. Thus, the three-dimensional correlation function for the vertical turbulent component is defined as

$$R_w(\boldsymbol{x}_1, \boldsymbol{x}_2) = \langle w(\boldsymbol{x}_1) w(\boldsymbol{x}_2) \rangle, \tag{A 1}$$

where $w(\boldsymbol{x}_1)$ and $w(\boldsymbol{x}_2)$ are the vertical turbulent fluctuations at the two points, and the angle brackets indicate ensemble average. By definition, in homogeneous turbulence, the correlation function depends only on the spatial separation between $\boldsymbol{x}_1$ and $\boldsymbol{x}_2$. Hence, we may write

$$R_w(\boldsymbol{r}) = \langle w(\boldsymbol{x}_1) w(\boldsymbol{x}_2) \rangle, \tag{A 2}$$

where $\boldsymbol{r} = (\Delta x,\ \Delta y,\ \Delta z) = \boldsymbol{x}_1 - \boldsymbol{x}_2$, with Δx, Δy, Δz in the x, y and z directions, respectively.

The spectra are Fourier transforms of the correlation function. For example, the one-wavenumber cross-spectrum is

$$S_w(k_1,\ \Delta y,\ \Delta z) = 2\sigma_w^2 \int_{-\infty}^{\infty} R_w(\Delta x,\ \Delta y,\ \Delta z)\exp(-\mathrm{i}2\pi k_1 \Delta x)\,\mathrm{d}\Delta x, \tag{A 3}$$

where σ_w is defined as in (3.1). The ordinary, one-point, spectrum would be $S_w(k_1,\ 0,\ 0)$. A cross-spectrum can be considered a mixed spatial correlation/spectral function.

In addition to the one-wavenumber spectrum, the two- and three-wavenumber spectra can be defined similarly as follows:

$$\begin{aligned} S_w(k_1,\ k_2,\ \Delta z) &= 2\sigma_w^2 \int_{-\infty}^{\infty} R_w(\Delta x,\ \Delta y,\ \Delta z)\exp[-\mathrm{i}(2\pi k_1 \Delta x + 2\pi k_2 \Delta y)]\,\mathrm{d}\Delta x\,\mathrm{d}\Delta y \\ &= \int_{-\infty}^{\infty} S_w(k_1,\ \Delta y,\ \Delta z)\exp(-\mathrm{i}2\pi k_2 \Delta y)\,\mathrm{d}\Delta y, \end{aligned} \tag{A 4}$$

$$\begin{aligned} S_w(k_1,\ k_2,\ k_3) &= 2\sigma_w^2 \int_{-\infty}^{\infty} R_w(\Delta x,\ \Delta y,\ \Delta z) \\ &\quad \times \exp[-\mathrm{i}(2\pi k_1 \Delta x + 2\pi k_2 \Delta y + 2\pi k_3 \Delta z)]\,\mathrm{d}\Delta x\,\mathrm{d}\Delta y\,\mathrm{d}\Delta z \\ &= \int_{-\infty}^{\infty} S_w(k_1,\ \Delta y,\ \Delta z)\exp[-\mathrm{i}(2\pi k_2 \Delta y + 2\pi k_3 \Delta z)]\,\mathrm{d}\Delta y\,\mathrm{d}\Delta z \\ &= \int_{-\infty}^{\infty} S_w(k_1,\ k_2,\ \Delta z)\exp(-\mathrm{i}2\pi k_3 \Delta z)\,\mathrm{d}\Delta z. \end{aligned} \tag{A 5}$$

It should be noted that these spectra can be expressed in terms of one-point spectra and a corresponding coherence function as in (2.8). Using the inverse Fourier transform, the correlation function can be obtained from the turbulence spectra. Hence, only one of these functions is independent because of the Fourier transform interrelationships (Etkin 1971).

A.2. *Cross-spectrum of lift on a thin aerofoil*

Based on Ribner's three-wavenumber spectral model, the cross-spectrum of the lift on thin aerofoil can be derived using the two-dimensional inverse Fourier transform of (2.1), which is given by

$$\begin{aligned} S_L(k_1,\ \Delta y,\ \Delta z) &= (\rho U b C_L')^2 \int\int_{-\infty}^{\infty} |\chi_L(k_1,\ k_2,\ k_3)|^2 S_w(k_1,\ k_2,\ k_3) \\ &\quad \times \exp[2\pi\mathrm{i}(k_2 \Delta y + k_3 \Delta z)]\,\mathrm{d}k_2\,\mathrm{d}k_3, \end{aligned} \tag{A 6}$$

where $S_L(k_1,\ \Delta y,\ \Delta z)$ is the cross-spectrum of the lift force between two spatial locations separated by Δy in the spanwise direction and by Δz in the vertical direction.

The Fourier transform of the product of the two functions is given by (Bracewell 1978)

$$\mathcal{F}[f(t)g(t)] = \frac{1}{2\pi} F(\omega) \otimes G(\omega), \tag{A 7}$$

where '$\mathcal{F}$' is the Fourier transform operator, $\mathcal{F}[f(t)] = F(\omega)$, $\mathcal{F}[g(t)] = G(\omega)$, and '$\otimes$' is the one-dimensional convolution operator. By introducing the two-dimensional convolution as in (A 7), (A 6) can be rewritten as follows:

$$S_L(k_1, \Delta y, \Delta z) = (\rho U b C_L')^2 |\chi_L(k_1, \Delta y, \Delta z)|^2 \otimes\otimes S_w(k_1, \Delta y, \Delta z), \tag{A 8}$$

where '$\otimes\otimes$' denotes the two-dimensional convolution operation, $|\chi_L(k_1, \Delta y, \Delta z)|^2$ and $S_w(k_1, \Delta y, \Delta z)$ are the two-dimensional inverse Fourier transforms of $|\chi_L(k_1, k_2, k_3)|^2$ and $S_w(k_1, k_2, k_3)$, respectively. Similarly to the cross-spectrum of the vertical velocity fluctuations, $|\chi_L(k_1, \Delta y, \Delta z)|^2$ is defined as the cross-3D admittance, which can describe the variations of the 3D AAF between two spatial locations.

Equation (A 8) indicates that the cross-spectrum of the lift force should be represented as the convolution between the cross-3D admittance and the cross-spectrum of the w component instead of the product of $|\chi_L(k_1, \Delta y, \Delta z)|^2$ and $S_w(k_1, \Delta y, \Delta z)$ directly. If the spatial correlation of the lift in the vertical direction is negligible, then (A 8) is simplified to

$$S_L(k_1, \Delta y) = (\rho U b C_L')^2 |\chi_L(k_1, \Delta y)|^2 \otimes S_w(k_1, \Delta y), \tag{A 9}$$

where the cross-3D admittance $|\chi_L(k_1, \Delta y)|^2$ is

$$|\chi_L(k_1, \Delta y)|^2 = \int_{-\infty}^{\infty} |\chi_L(k_1, k_2)|^2 \exp(\mathrm{i}k_2 \Delta y)\, \mathrm{d}k_2. \tag{A 10}$$

Moreover, $S_w(k_1, \Delta y)$ can be expressed as the product of the coherence and the one-point spectrum, which gives

$$S_w(k_1, \Delta y) = \mathrm{Coh}_w(k_1, \Delta y) S_w(k_1), \tag{A 11}$$

where $\mathrm{Coh}_w(k_1, \Delta y)$ is the coherence of the vertical velocity fluctuations in the spanwise direction. By substituting (A 11) into (A 9), $S_L(k_1, \Delta y)$ can be defined by a one-dimensional convolution

$$S_L(k_1, \Delta y) = (\rho U b C_L')^2 [|\chi_L(k_1, \Delta y)|^2 \otimes \mathrm{Coh}_w(k_1, \Delta y)] S_w(k_1). \tag{A 12}$$

Appendix B

B.1. *Mugridge's 3D AAF model*

Compared with Graham's exact function, Mugridge's 3D AAF is of high accuracy with respect to $k_1 < 1/\pi$ and can be written as

$$|\chi_L(k_1, k_2)|^2 = \underbrace{\frac{1}{1 + 2\pi\tilde{k}_1}}_{\textit{Sears' fun.}} \underbrace{|F_L(k_1, k_2)|^2}_{\textit{correction fac.}}, \tag{B 1}$$

where $|F_L(k_1, k_2)|^2$ is the correction factor for describing the spanwise variations of the lift force, which is given by

$$|F_L(k_1, k_2)|^2 = \frac{\lambda_L^2}{\lambda_L^2 + k_2^2}, \tag{B 2}$$

with

$$\lambda_L = \sqrt{\tilde{k}_1^2 + 2/\pi^2}/(2\pi b), \tag{B 3}$$

where $\tilde{k}_1 = 2\pi k_1 b$.

B.2. *Blake's 3D AAF model*

Blake's approximation has the same form as (B 1) and (B 2) but with the parameter λ_L replaced by

$$\lambda_L = \frac{\sqrt{[1 + 3.2(2\tilde{k}_1)^{1/2}]/9.6}}{(2\pi b)}. \tag{B 4}$$

B.3. *The cross-3D admittance*

Based on Mugridge's or Blake's approximations, the cross-3D admittance can be obtained by substituting (B 1) and (B 2) into (A 10), which yields

$$|\chi_L(k_1, \Delta y)|^2 = \frac{\pi\lambda_L}{1 + 2\pi\tilde{k}_1}\,\mathrm{Coh}_{\chi_L}(k_1, \Delta y) \tag{B 5}$$

and the coherence of 3D AAF is given by

$$\mathrm{Coh}_{\chi_L}(k_1, \Delta y) = \exp(-2\pi\lambda_L \Delta y), \tag{B 6}$$

where λ_L is defined by (B 3) or (B 4).

Appendix C

The improved Jakobsen's empirical coherence model is given by

$$\mathrm{Coh}_w(k_1, \Delta y) = \exp(-2\pi A_w \Delta y), \tag{C 1}$$

where

$$A_w = \left[\sqrt{c_2^2 + (c_3 k_1 L_w^x)^2}\right]^{c_1} / (2\pi L_w^x); \tag{C 2}$$

c_1, c_2, c_3 are kept as floating parameters for the least-squares fits, and L_w^x is the integral length scale of vertical velocity fluctuations. The two-wavenumber coherence of (C 1) is obtained by using the inverse Fourier transform

$$\begin{aligned}\Phi_w(k_1, k_2) &= \int_{-\infty}^{\infty} \mathrm{Coh}_w(k_1, \Delta y)\exp(\mathrm{i}k_2\Delta y)\,\mathrm{d}\Delta y \\ &= \frac{1}{\pi}\frac{A_w}{(A_w^2 + k_2^2)}.\end{aligned} \tag{C 3}$$

Appendix D

To validate the closed-form expression of the lift cross-spectrum in (2.3)–(2.7), the relationship between the one- and two-wavenumber spectra of the lift force is applied, which is defined as

$$S_L(k_1) = \int_{-\infty}^{\infty} S_L(k_1, k_2)\,\mathrm{d}k_2. \tag{D 1}$$

If the thin aerofoil is regarded as a lift-surface, $S_L(\boldsymbol{k})$ is a function of only two wavenumbers. Hence, equation (2.1) becomes

$$S_L(k_1, k_2) = (\rho U b C_L')^2 |\chi_L(k_1, k_2)|^2 S_w(k_1, k_2), \tag{D 2}$$

where

$$S_w(k_1, k_2) = \Phi_w(k_1, k_2) S_w(k_1). \tag{D 3}$$

Substituting (B 1), (B 2) and (C 3) into (D 3), the two-wavenumber lift spectrum is given by

$$S_L(k_1, k_2) = (\rho U b C_L')^2 \left(\frac{1}{1 + 2\pi\tilde{k}_1} \frac{\lambda_L^2}{\lambda_L^2 + k_2^2} \right) \left[\frac{1}{\pi} \frac{A_w}{A_w^2 + k_2^2} S_w(k_1) \right]. \tag{D 4}$$

Substituting (D 4) into (D 1), the generalized one-wavenumber lift spectrum can be obtained by using the following infinite integral relation

$$\int_0^\infty \frac{\mathrm{d}x}{(\beta + x^2)(\gamma + x^2)} = \frac{\pi}{2(\gamma - \beta)} \left(\frac{1}{\sqrt{\beta}} - \frac{1}{\sqrt{\gamma}} \right). \tag{D 5}$$

The result is in accord with those presented in (2.5)–(2.7), which suggests that the closed-form formulation of the lift cross-spectrum in (2.3)–(2.4) is valid.

Nomenclature

a_1, a_2, a_3	Floating parameters in λ_L
A_w	Decay parameter in Jakobsen's coherence model
b	Semi-chord length
C_D	Static coefficient of drag
C_L	Static coefficient of lift
C_L'	Lift slope
$\mathrm{Coh}_L(k_1, \Delta y)$	Coherence of lift force
$\mathrm{Coh}_w(k_1, \Delta y)$	Coherence of vertical velocity fluctuations
$\mathrm{Coh}_{\chi_L}(k_1, \Delta y)$	Coherence of three-dimensional aerodynamic admittance
$\lvert F_L(k_1, k_2)\rvert^2$	Correction factor of three-dimensional aerodynamic admittance
$\lvert F_L(k_1)\rvert^2$	Correction factor of generalized one-wavenumber admittance
$\boldsymbol{k}$	Three-dimensional wavevector
$\tilde{k}_1$	Non-dimensional chordwise wavenumber ($\tilde{k}_1 = 2\pi n b/U$), reduced frequency
k_1, k_2, k_3	Wavenumber in x, y, z directions respectively
$L^y(k_1)$	Correlation length scales
L^y	Correlation width
L_1, L_2	The lift on strip 1 and 2 along the span of the body
L_u^x, L_w^x, L_v^x	Integral length scales of u, v, w with respect to streamwise direction
n_1	Spanwise frequency
$R_{L,w}$	Correlation coefficients
$S_L(k_1)$	One-point spectrum of lift
$S_L(k_1, k_2)$	Two-wavenumber spectrum of lift
$S_L(k_1, \Delta y)$	Cross-spectrum of lift
$S_w(k_1)$	One-point spectrum of vertical velocity fluctuations
$S_w(k_1, k_2)$	Two-wavenumber spectrum of vertical velocity fluctuations
$S_w(k_1, \Delta y)$	Cross-spectrum of vertical velocity fluctuations
U	Mean wind velocity
w	Vertical velocity fluctuations

x, y, z	Chordwise, spanwise and vertical coordinates
Γ	Gamma function
Δ_{Coh}	Difference between coherence of lift and $w(=\mathrm{Coh}_L - \mathrm{Coh}_w)$
λ_L	Decay parameter in coherence of 3D aerodynamic admittance
ρ	Air density
σ_w	RMS of vertical velocity fluctuations
$\Phi_w(k_1, k_2)$	Two-wavenumber coherence of vertical velocity fluctuations
$\Phi_L(k_1, k_2)$	Two-wavenumber coherence of lift
$\lvert\chi_L(k_1)\rvert^2$	Generalized one-wavenumber admittance
$\lvert\chi_L(k_1, k_2)\rvert^2$	Three-dimensional aerodynamic admittance (two-wavenumber)
$\lvert\chi_L(k_1, \Delta y)\rvert^2$	Cross-3D admittance
$\lvert\chi_L(k_1, 0)\rvert^2$	Two-dimensional aerodynamic admittance in two-dimensional flow
$\Psi_L(k_1, \Delta y)$	Equivalent coherence of lift force

REFERENCES

BATCHELOR, G. K. 1959 *The Theory of Homogeneous Turbulence*. pp. 1–2. Cambridge University Press.

BEARMAN, P. W. 1971 An investigation of the forces on flat plates normal to a turbulent flow. *J. Fluid Mech.* **46**, 177–198.

BEARMAN, P. W. 1972 Some measurements of the distortion of turbulence approaching a two-dimensional bluff body. *J. Fluid Mech.* **53**, 451–467.

BLAKE, W. K. 1986 Noncavitating lifting sections. In *Mechanics of Flow-induced Sound and Vibration* (ed. F. N. Frenkiel & G. Temple), p. 743. Academic.

BRACEWELL, R. N. 1978 *The Fourier Transform and Its Applications* (ed. R. N. Bracewell), pp. 154–243. McGraw-Hill.

CHERRY, N. J., HILLER, R. & LATOUR, M. E. M. P. 1984 Unsteady measurements in a separated and reattaching flow. *J. Fluid Mech.* **144**, 13–46.

DAVENPORT, A. G. 1962 Buffeting of a suspension bridge by storm winds. *J. Struct. Div.* **88**, 233–270.

ETKIN, B. 1971 Flight in a turbulent atmosphere. In *Dynamic of Atmospheric Flight* (ed. B. Etkin), pp. 531–539. Wiley.

FILOTAS, L. T. 1969*a* Theory of airfoil response in a gusty atmosphere. Part I-Aerodynamic transfer function. *Tech. Rep.* 139. UTIAS Rep.

FILOTAS, L. T. 1969*b* Theory of airfoil response in a gusty atmosphere. Part II-Reponse to discrete gusts or continuous turbulence. *Tech. Rep.* 141. UTIAS Rep.

FUNG, Y. C. 1969 *An Introduction to the Theory of Aeroelasticity* (ed. Y. C. Fung), p. 35. Dover.

GRAHAM, J. M. 1970 Lifting-surface theory for the problem of an arbitrary yawed sinusoidal gust incident on a thin aerofoil in incompressible flow. *Aeronaut. Q.* **21**, 182–198.

GRAHAM, J. M. 1971 A lift-surface theory for the rectangular wing in non-stationary flow. *Aeronaut. Q.* **22**, 83–100.

HANN, F. L., WU, T. & KAREEM, A. 2016 Correlation structures of pressure field and integrated forces on oscillating prism in turbulent flows. *J. Engng Mech. ASCE* **142**, 0416017.

HJORTH-HANSEN, E., JAKOBSEN, A. & STRØMMEN, E. 1992 Wind buffeting of a rectangular box girder bridge. *J. Wind Engng Ind. Aerodyn.* **41–44**, 1215–1226.

IRWIN, H. P. A. H. 1977 Wind tunnel and analytical investigation of the response of Lion's Gate Bridge to turbulent wind. *Tech. Rep.* 210. NAE LTR-LA Rep.

ITO, Y., SHIRATO, H. & MATSUMOTO, M. 2014 Coherence characteristics of fluctuating lift forces for rectangular shape with various fairing decks. *J. Wind Engng Ind. Aerodyn.* **135**, 34–128.

JACKSON, R., GRAHAM, J. M. & MAULL, D. J. 1973 The lift on a wing in a turbulent flow. *Aeronaut. Q.* **24**, 155–166.

JAKOBSEN, J. B. 1997 Span-wise structure of lift and overturning moment on a motionless bridge girder. *J. Wind Engng Ind. Aerodyn.* **69–71**, 795–805.

KIMURA, K., FUJINO, Y., NAKATO, S. & TAMURA, H. 1997 Characteristics of buffeting forces on flat cylinders. *J. Wind Engng Ind. Aerodyn.* **69–71**, 365–374.

KIYA, M. & SASAKI, K. 1983 Structure of a turbulent separation bubble. *J. Fluid Mech.* **137**, 82–113.

KIYA, M. & SASAKI, K. 1985 Structure of large-scale vortices and unsteady reverse flow in the reattaching zone of a turbulent separation bubble. *J. Fluid Mech.* **154**, 463–491.

LAROSE, G. L. 1997 The dynamic action of gusty winds on long-span bridges. PhD thesis, Technical University of Denmark.

LAROSE, G. L. & MANN, J. 1998 Gust loading on streamlined bridge decks. *J. Fluids Struct.* **12**, 511–536.

LI, S. 2015 Characteristics of buffeting forces on rectangular cylinder and streamlined box girder. PhD thesis, Southwest Jiaotong University.

LI, S., LI, M. & LIAO, H. 2015 The lift on an aerofoil in grid-generated turbulence. *J. Fluid Mech.* **771**, 16–35.

LIEPMANN, H. W. 1955 Extension of the statistical approach to buffeting and gust response of wings of finite span. *J. Aero. Sci.* **22**, 197–200.

MA, C. 2007 3-d aerodynamic admittance research of streamlined box bridge decks. PhD thesis, Southwest Jiaotong University.

MANN, J. 1994 The spatial structure of netural atmospheric surface-layer turbulence. *J. Fluid Mech.* **273**, 141–168.

MASSARO, M. & GRAHAM, J. M. R. 2015 The effect of three-dimensionality on the aerodynamic admittance of thin sections in free stream turbulence. *J. Fluids Struct.* **57**, 81–89.

MUGRIDGE, B. D. 1970 The generation and radiation of acoustic energy by the blades of a subsonic axial flow fan due to unsteady flow interaction. PhD thesis, University of Southampton.

MUGRIDGE, B. D. 1971 Gust loading on a thin aerofoil. *Aeronaut. Q.* **22**, 301–310.

NAKAMURA, Y. & OZONO, S. 1987 The effects of turbulence on a separated and reattaching flow. *J. Fluid Mech.* **178**, 477–490.

RIBNER, H. S. 1956 Spectral theory of buffeting and gust response: unification and extension. *J. Aero. Sci.* **23**, 1075–1077.

ROBERTS, J. B. & SURRY, D. 1973 Coherence of grid-generated turbulence. *J. Engng Mech. Div.* **99**, 1227–1245.

SANKARAN, R. & JANCAUSKAS, E. D. 1993 Measurements of cross-correlation in separated flows around bluff cylinders. *J. Wind Engng Ind. Aerodyn.* **49**, 279–288.

TAYLOR, J. 1965 Theoretical analysis of turbulence. In *Manual on Aircraft Loads* (ed. J. Taylor), pp. 200–203. Pergamon.

YAN, L., ZHU, L. & FLAY, R. G. J. 2016 Span-wise correlation of wind-induced fluctuating forces on a motionless flat-box bridge deck. *J. Wind Engng Ind. Aerodyn.* **156**, 115–128.